Insights into magma dynamics from daily OP-FTIR gas compositions throughout the 2021 Tajogaite eruption, La Palma, Canary Islands

María Asensio-Ramos, Ana Pardo Cofrades, Mike Burton, Alessandro La Spina, Patrick Allard, José Barrancos, Catherine Hayer, Ben Esse, Luca D'auria, Pedro A Hernández, et al.

Chemical Geology 676 (2025) 122605

Contents lists available at ScienceDirect

Chemical Geology

journal homepage: www.elsevier.com/locate/chemgeo

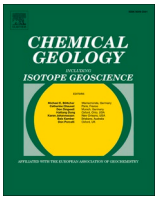

Insights into magma dynamics from daily OP-FTIR gas compositions throughout the 2021 Tajogaite eruption, La Palma, Canary Islands

María Asensio-Ramos [a,1,*], Ana Pardo Cofrades [b,1], Mike Burton [b,c,d], Alessandro La Spina [d], Patrick Allard [d,e], José Barrancos [a,f], Catherine Hayer [b,g], Ben Esse [b], Luca D'Auria [a,h], Pedro A. Hernández [a,h], Eleazar Padrón [a,h], Gladys V. Melián [a,h], Nemesio M. Pérez [a,h]

[a] Instituto Volcanológico de Canarias (INVOLCAN), 38320, Puerto de la Cruz, Tenerife, Canary Islands, Spain
[b] University of Manchester, Department of Earth and Environmental Science, Manchester, United Kingdom
[c] Centre for Observation and Modelling of Earthquakes, Volcanoes and Tectonics (COMET), United Kingdom
[d] Istituto Nazionale di Geofisica e Vulcanologia (INGV), Sezione di Catania, Italy
[e] Université Paris Cité, Institut de Physique du Globe de Paris, France
[f] Grupo de Observación de la Tierra y la Atmósfera (GOTA), Universidad de La Laguna, Avda. Astrofísico Francisco Sánchez s/n, 38200, La Laguna, Tenerife, Spain
[g] Hamtec Consulting at EUMETSAT, Germany
[h] Instituto Tecnológico y de Energías Renovables (ITER), 38600 Granadilla de Abona, Tenerife, Canary Islands, Spain

ARTICLE INFO

Editor: Dr. Claudia Romano

Keywords:
Canary Islands
Cumbre Vieja
Geochemistry
Magma degassing
La Palma
OP-FTIR
Volcanic eruption

ABSTRACT

From September 19 to December 12, 2021, a mixed explosive-effusive eruption impacted La Palma Island, in the Canary archipelago, leading to the growth of Tajogaite volcanic cone. Daily Open-Path Fourier Transform Infrared (OP-FTIR) measurements from October 3 until the end of the eruption allowed us to capture the molar proportions of H_2O, CO_2, SO_2, HCl and CO (plus COS occasionally) in magmatic gases emitted from summit and flank vents of the new cone. Our results reveal high CO_2/SO_2 ratios ranging from 11 to 53 in explosive gas emissions throughout most of the eruption, with a time-averaged value of ~30. In contrast, effusive degassing at lower flank vents systematically displayed lower CO_2/SO_2 ratios (from 3 to 11) and enhanced proportions of H_2O, S and Cl. Combined with solubility data and the magma eruption rates, this chemical contrast suggests gas fractionation in a very shallow conduit branching beneath the Tajogaite cone, were most of the pre-exsolved CO_2-rich gas phase but a minor fraction of the magma explosively escaped through the main eruptive conduit, while CO_2-depleted gas and most of the magma were effusively discharged through lateral branches. The $CO/COS/CO_2$ ratios for explosive degassing are consistent with petrological evidence of oxidized magmatic conditions (FMQ $+1.7 \pm 0.3$), which enhanced sulfur solubility and late-stage SO_2 outgassing. The high oxidation state, as well as low HCl/HF ratios, retrieved from solar occultation across the volcanic plume, are both typical of Ocean Island Basalt (OIB) magmatism. The apparent increase of CO_2/SO_2 and SO_2/HCl ratios at summit vents during the first half of the eruption is consistent with the influx of progressively more mafic, deeper-derived, basanitic magma, though we cannot entirely rule out artefacts due to more challenging measurement of the pure explosive gas in that period. Our study presents the very first detailed data set for gas geochemistry during a subaerial eruption in the Canary archipelago and highlights the remarkable potential of OP-FTIR spectroscopy for real-time monitoring and study of volcanic eruptions.

1. Introduction

Measuring magmatic gas compositions during a volcanic eruption can provide crucial insights into the dynamics of magma ascent and the processes that determine eruptive styles. This relies on the contrasting solubility/degassing behaviour of magmatic volatiles upon decompression and the capability of gas bubbles to uprise separately from their host magma, thereby preserving the record of underground pressure-temperature-redox (P-T-redox) conditions (Giggenbach, 1996). In addition, magma transit through shallow conduit plumbing systems can

* Corresponding author.
E-mail address: maria.asensio@involcan.org (M. Asensio-Ramos).
[1] María Asensio-Ramos and Ana Pardo Cofrades share first authorship of this manuscript, as they have contributed equally.

https://doi.org/10.1016/j.chemgeo.2024.122605
Received 6 June 2024; Received in revised form 25 December 2024; Accepted 27 December 2024
Available online 3 January 2025

play a key role in controlling gas compositions and fluxes, due to partitioning of gas and magma between different conduits (La Spina et al., 2010).

Magmatic volatiles (H_2O, CO_2, S, Cl, F in typical decreasing order of abundance) have contrasted pressure-related solubility behaviors. CO_2 is by far the least soluble and the first to form gas bubbles in magma, even at great depth (e.g., Holloway and Blank, 1994; Blank and Brooker, 2018), whereas highly soluble species like Cl and F rarely reach saturation and partition into the co-existing fluid phase at relatively shallow depth (e.g., Carrol and Webster, 1994; Spilliaert et al., 2006; Baker and Alletti, 2012). H_2O and S usually display intermediate behaviors, depending on their initial abundances and, for sulfur, on the magma redox conditions (e.g., Baker and Moretti, 2011; Baker and Alletti, 2012). In addition to P-T-redox conditions, the composition of the magmatic gas phase can also be influenced by melt crystallization and interactions with hydrothermal systems, especially in volcanic island settings. Magma crystallization at depth can trigger volatile saturation, gas-melt partitioning, and the formation of magmatic brines enriched in NaCl, S and trace metals at the origin of some porphyry ore deposits (e.g., Giggenbach et al., 2005; Blundy et al., 2015; Ranta et al., 2020).

The composition of the exsolved magmatic gas phase evolves significantly as magma ascends. Gas bubbles, due to their higher buoyancy, can separate from their host melt, especially in low-viscosity mafic melts, and either migrate upward or/and accumulate as foams at discontinuities of magma feeding systems (e.g., Jaupart and Vergniolle, 1988; Sparks et al., 1994). Gas accumulation at shallow depths (e.g. < 3 km) can play a key role in controlling eruptive activity (Allard et al., 2005). During the rapid ascent of low viscosity magmas from greater depths (e.g. >10 km) the opportunity for *syn*-eruptive decoupling of gas and magma is more limited (Bamber et al., 2024) unless a branch in the feeding system is encountered. There, exsolved gas and magma may partition independently into branched conduits, generating gas emissions with distinct composition at different vents (e.g., Aiuppa et al., 2002; Burton et al., 2003; La Spina et al., 2010). This was clearly observed, for instance, during passive degassing at the summit craters of Mt. Etna, where central conduit emissions displayed a high CO_2/SO_2 ratio while simultaneous emissions from a peripheral vent fed by partly degassed magma displayed low CO_2/SO_2 ratios (La Spina et al., 2010). Measuring gas fluxes and compositions from each vent permits the depth and extent of gas-magma partitioning between the branches to be quantified.

Hence, measuring the chemical composition of volcanic gases during an eruption can provide detailed insights into the dynamics of magma ascent dynamics, the depth and extent of any gas-melt separation, and the geometry of the plumbing system itself. Temporal changes in gas compositions during an eruption can help assess the evolution of these parameters and their control of eruptive styles. This information is an extremely valuable resource for volcanological research but also for hazard assessment before and during eruptive events.

Measuring the composition of volcanic gases during an eruption, however, remains a challenging task, due to instrumental and logistical difficulties, as well as safety concerns. Over the past two decades, open-path Fourier transform infrared (OP-FTIR) spectroscopy has been demonstrated to be a highly effective tool for remotely quantifying magmatic gas compositions during eruptions, by analysing absorption spectra of the infrared radiation emitted by molten lava (e.g., Allard et al., 2005; Burton et al., 2007; Oppenheimer and Kyle, 2008; Sawyer et al., 2008; Allard et al., 2010; La Spina et al., 2015; Allard et al., 2016b; Burton et al., 2023; Scott et al., 2023). OP-FTIR absorption spectroscopy allows simultaneous high frequency analysis of the primary components of magmatic gas (H_2O, CO_2, SO_2, HCl, HF and CO, though not H_2 and H_2S) from a safe distance. When the quality of OP-FTIR spectra allows it, some other minor species of special interest for thermodynamic computations, such as COS, can also be quantified (e.g. Burton et al., 2007; Oppenheimer et al., 2018). During an eruption with multiple vents, this technique can be used to distinguish the chemistry of gas emissions produced from each vent. As such, OP-FTIR absorption spectroscopy has opened a new era for studying and monitoring magma degassing processes during volcanic eruptions. Operating this tool on volcanoes typically requires a clear view of eruptive jets/columns and a radiation source hotter than the target gas phase. Variations in gas temperature, mixing with atmospheric gases and other possible gas sources along the viewing pathlength between the radiation source and the spectrometer, as well as the density of ash particles in the gas plume, can all influence spectral retrieval of volcanic gas species and, hence, must be taken into consideration (La Spina et al., 2015).

Here we report the chemical composition of magmatic gas emissions measured daily with OP-FTIR spectroscopy during the 2021 Tajogaite eruption of the Cumbre Vieja volcanic system, on La Palma Island in the Canary archipelago (Spain). The results for both explosive and effusive activities during the eruption allow us to discuss the magma degassing processes which controlled the dynamics of this remarkable event. Our study provides not only the very first detailed dataset for magmatic gases during a subaerial eruption in the Canary Islands, but also offers the most comprehensive description of the chemical evolution of magma degassing throughout an entire volcanic eruption.

2. Geologic setting and 2021 Tajogaite eruption

La Palma is one of the seven main volcanic islands composing the Canary archipelago, located off the north-western coast of Africa in the eastern Atlantic Ocean (**Fig. 1A**). These islands represent the subaerial parts of a group of voluminous intra-plate oceanic volcanoes that produce alkaline magmas and whose age decreases westward (Carracedo et al., 2001; Schmincke and Sumita, 2004). La Palma and El Hierro, the two westernmost islands, are the youngest and the most active volcanic centers of the archipelago. La Palma volcanic complex is composed of a 3300 km^3 submarine part, raising ca. 4000 m above the ocean floor and built over the past 4 Ma, and a $\sim$ 600 km^3 subaerial part reaching 2426 m above sea level that has been growing for 1.7 Ma (Staudigel and Schmincke, 1984; Masson et al., 2002). It thus ranks among the tallest volcanic edifices on the planet. Subaerial eruptive activity first formed the Taburiente shield volcano that makes a large northern part of the island (Guillou et al., 2001; Staudigel et al., 1986). The subsequent southward formation of the Cumbre Nueva edifice was associated with a spectacular flank collapse, about 0.5 million years ago, which created the Caldera de Taburiente and led to the emergence of the Bejenado stratovolcano. Cumbre Vieja, the most recent and the most active volcanic edifice, occupies over 220 km^2 in the southern part of La Palma. It is a polygenetic volcano aligned along a N-S ridge and composed of thick mafic lava flows, Strombolian and phreatomagmatic basaltic cones, as well as some phonolithic domes (Navarro and Coello, 1993; Ancochea et al., 1994; Carracedo et al., 1999). Prior to the 2021 Tajogaite eruption, the Cumbre Vieja system had produced seven historic eruptions, between 1470 and 1492 (Tacande), in 1585 (Tahuya), 1646 (Tigalate), 1677 (San Antonio), 1712 (El Charco), 1949 (San Juan), and ultimately in 1971 (Teneguía).

The 2021 eruption of Cumbre Vieja was preceded by several signs of unrest, including subtle yet measurable ground deformation starting in 2009 (Fernández et al., 2021), series of seismic swarms in 2017–2020 following 46 years of seismic quiescence (Torres-González et al., 2020; D'Auria et al., 2022), and geochemical anomalies in soil gas emanations and groundwaters since 2010 (Padrón et al., 2015, 2022; Amonte et al., 2023). Seismicity escalated from September 11, 2021, with an upward migration of hypocenters, indicating rapid magma ascent from ca. 10 km depth towards the surface (D'Auria et al., 2022). The eruption started on September 19 along a SE-NW fracture system at elevation of 800–1100 m above sea level and approximately 1.6 km northeast of the El Paraíso neighborhood of El Paso municipality (Romero et al., 2022). Initially, five vents opened along that fracture system but, after a few days, the eruption rapidly concentrated at downslope main vents where the new volcanic cone, Tajogaite, started to form. The most energetic activities at

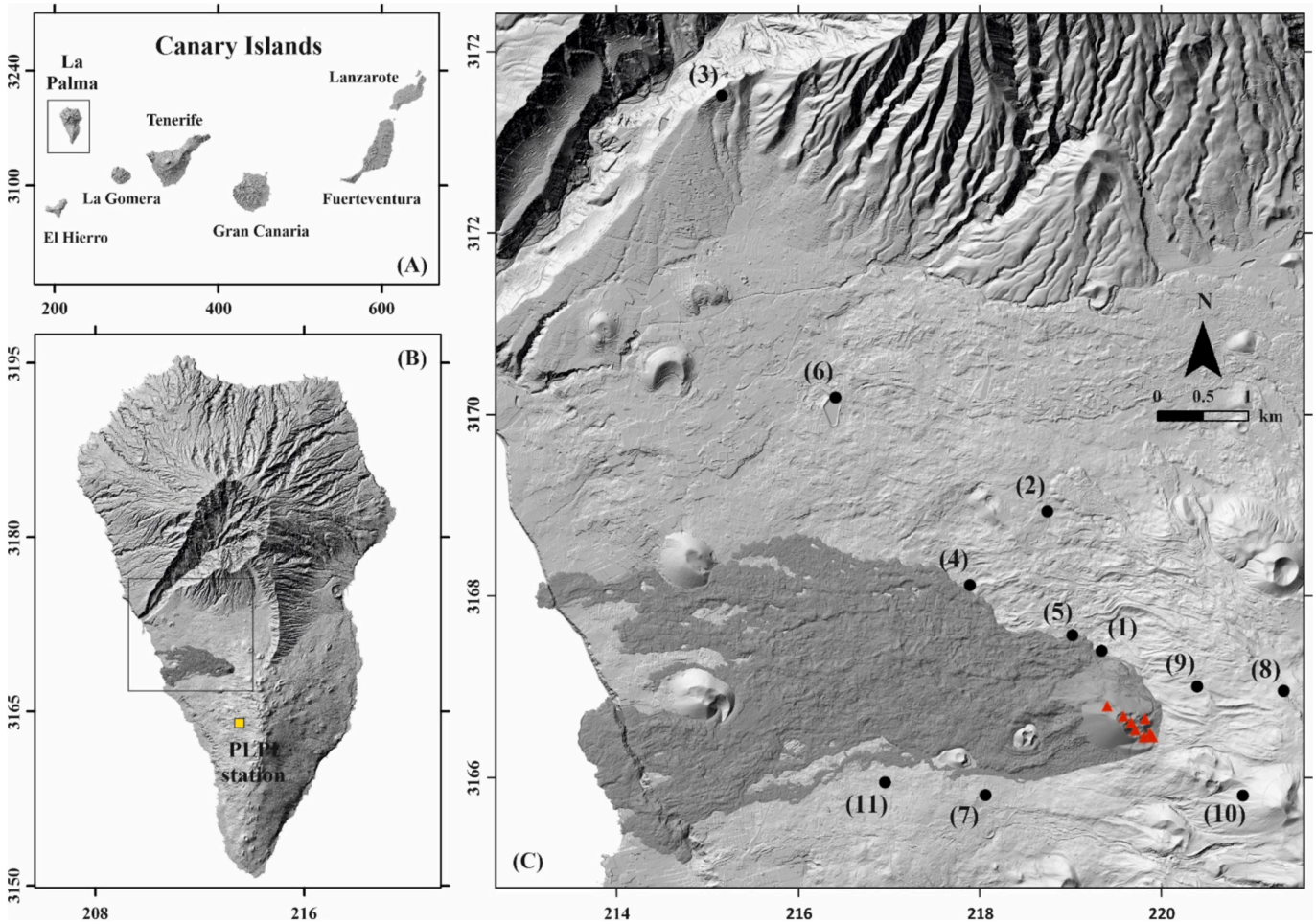

Fig. 1. **(A)** Location of La Palma Island in the Canary Archipelago. **(B)** Location of the area affected by the eruption on the western flank of Cumbre Vieja volcano and location of PLPI seismic station. **(C)** Zoomed map of the lava flows area and location of the upper eruptive vents (red triangles). Black solid dots indicate our OP-FTIR measurement sites: **(1)** Tacande 1, **(2)** Tacande 2, **(3)** Villa José, **(4)** Tajuya, **(5)** Tacande 3, **(6)** Dos Pinos, **(7)** Las Manchas 1, **(8)** Mirador Astronómico del Llano del Jable, **(9)** Cabeza de Vaca, **(10)** Pista forestal Fran Santana, **(11)** Las Manchas 2.

the upper vents of this cone alternated between lava fountaining, pulsated Strombolian explosions and sustained ash emissions, which produced dense ash columns and tephra fallouts. In contrast, eruptive activity at the lower flank vents on the W-SW side of the Tajogaite cone was characterized by persistent, steady, lava spattering and effusion of abundant lava flows. This mixed explosive-effusive activity continued during most of the eruption, though with intermittent variations in intensity and rapid transitions in eruptive styles, as the cone grew. By the time the eruption ended on December 13, 2021, the newly formed Tajogaite cone was 187 m high and had a volume of 36.5 ± 0.3 million m^3 (Civico et al., 2022).

With a total duration of 85 days, a total volume of erupted material of 217.4 ± 6.6 Mm^3, including both lava flows (dense rock) and unconsolidated proximal fallout deposits (Civico et al., 2022) and a total measured SO_2, calculated by PlumeTraj, of 1.6 ± 0.1 Mtons (Esse et al., 2025), the 2021 Tajogaite eruption of Cumbre Vieja is the longest and largest historic volcanic event ever recorded in La Palma Island and one of the most important in Europe over the past 75 years. Its lava flows and lapilli-ash fallout heavily damaged the inhabited surroundings in the western part of the island. Lava flows covered more than 1200 ha, as seen in **Fig. 1B**, destroying nearly 3000 buildings and damaging approximately 90 km of road infrastructure (European Commission, Joint Research Centre (JRC) (2021): *Volcano eruption in La Palma, Spain (2021-09-19)*, (http://data.europa.eu/89h/6fc2d36e-890c-47b8-9f5f-662816238678)). More than 7000 people were forced to evacuate and a total cost of damage of over 900 million euros was estimated by local authorities. At the same time, this spectacular eruption in a densely populated area attracted the attention of tourists, volcano-enthusiasts, and media organizations, resulting in an unprecedented collection of imagery and videography captured at high spatial and temporal resolutions (Wadsworth et al., 2022).

3. Methodology

3.1. OP-FTIR measurements

We collected infrared spectra of the eruptive gases using two OP-FTIR spectrometers built by MIDAC Corporation (Westfield, MA, USA). Each spectrometer was equipped with a closed-cycle Stirling-engine-cooled MCT detector, which is sensitive between 800 and 5000 cm^{-1} and had a spectral resolution of 0.5 cm^{-1}. The field of view of the instruments was 20 mrad. The spectrometers were mounted on lightweight tripods and controlled by laptop PCs connected via an Ethernet cable using *Essential FTIR* software. Power was provided by 12 V batteries. Measurements were performed in passive mode, utilizing the infrared radiation emitted by both magma fragments in lava fountains and explosive jets, as well as molten lava flows.

We conducted OP-FTIR measurements on a nearly daily basis from October 3 to December 12, using different sites. Each measurement site was carefully selected every day based on the ongoing eruptive activity

and the best balancing between safety, proximity, and optimized geometry for OP-FTIR sensing. The measurement site could thus vary during the same day or across a specific area to account for changing eruptive conditions, wind direction, and the advance of lava flows. **Fig. 1C** shows the location of all sites, numbered in their chronological order of use, with corresponding specificities detailed in Table 1. On several occasions we could operate the two MIDAC spectrometers synchronously, from either the same site or different sites, which permitted us to measure the contemporaneous gas emissions from distinct vents.

Most of our FTIR spectra displayed gas absorption features, implying that the targeted gases were generally cooler than the magmatic radiation source as they were sensed. Spectra were analysed following the retrieval procedures developed for OP-FTIR spectrum analysis of high temperature volcanic gases (Allard et al., 2005; Burton et al., 2007; La Spina et al., 2015). The column amounts of the different gas species over the viewing path length were obtained through nonlinear least-squares best fitting between the measured spectra and synthetic spectra generated from a radiative transfer forward model (Edwards and Dudhia, 1996) and infrared absorption line parameters from the HITRAN database (Gordon et al., 2020). Radiative transfer was calculated in a two-layer model, the first layer containing air-diluted but hot volcanic gases and the second one purely atmospheric gas at ambient temperature (Burton et al., 2007). The volcanic gas layer temperature was set to 400 K, as estimated from best fitting in the temperature-sensitive $n_1 + n_3$ SO_2 absorption band centred on 2500 cm^{-1}. For CO_2 and H_2O, ambient temperature was assumed due to the significant atmospheric contribution to their total column amounts. These assumptions are consistent with prior studies (e.g., Burton et al., 2007). While the use of a fixed temperature (400 K) for SO_2 has proven robust for volcanic gas plumes with similar conditions, we note that variations in this parameter could lead to changes in the retrieved column amounts, particularly for species with strong temperature dependence in their absorption features. Similarly, assuming ambient temperature for CO_2 and H_2O simplifies the analysis but might introduce small biases in scenarios where plume-air mixing significantly alters local temperatures. For each spectrum we retrieved the path amounts (expressed in units of molecules/cm^2) of H_2O, CO_2, SO_2, HCl, CO, CH_4 and N_2O, using the spectral fitting windows listed in **Table 2**. Additionally, in a series of best spectra, we quantified COS in the 2030–2085 cm^{-1} window, applying an offset of 10 %. Uncertainty values for all retrieved species, including CO_2 and H_2O, are given in **Table 2**.

The choice of fitting windows is extremely important for retrieval accuracy, as it must account for the variability in volcanic and measurement conditions to optimize results for each spectral series. In our spectra from the Tajogaite eruption we observed strong interferencebetween H_2O and CO_2 absorptions in the 2030–2085 cm^{-1} window which is typicallyused to retrieve CO_2 (e.g., La Spina et al., 2015). To overcome this problem, we carried out extensive testing and found that CO_2 quantification was significantly improved by using the clearer and stronger CO_2 absorption features in the 2080 and 2150 cm^{-1} window.

Table 1
Specificities of the measuring sites.

Measuring site	*Name*	*Distance to upper vents (km)*
(1)	Tacande 1	0.7
(2)	Tacande 2	2.7
(3)	Villa José	8.4
(4)	Tajuya	2.4
(5)	Tacande 3	1.3
(6)	Dos Pinos	5.0
(7)	Las Manchas	1.8
(8)	Mirador Astronómico del Llano del Jable	1.8
(9)	Cabeza de Vaca	0.5
(10)	Pista forestal Fran Santana	1.5
(11)	Las Manchas	2.8

Table 2
Spectral fitting windows used for the analysis of each target gas (in bold). Due to their significant presence in the background, CO_2 and H_2O are considered in the atmospheric layer.

Volcanic gas	*Atmospheric gas*	*Window (wavenumber)*	*Mean relative error*
SO_2	H_2O	2450–2540	4–10 %
CO	**H_2O, CO_2**	2080–2150	10–15 %
HCl	H_2O, CH_4, N_2O	2690–2830	4–10 %
HF	H_2O	4033–4043	10–15 %
COS	CO, H_2O, CO_2	2030–2085	20 %

The error in the column amount for each species is determined by the standard deviation of fitting residuals across the respective spectral ranges (**Table 2**). While SO_2, HCl, HF and CO are purely or essentially volcanic in origin, H_2O and CO_2 are both volcanic and atmospheric components. To determine thevolcanic contribution of H_2O and CO_2, we used linear regression on scatter plots of H_2O and CO_2 against SO_2 or HCl, where the *y*-intercept represents the atmospheric background (e.g., Burton et al., 2000; Allard et al., 2016b). N_2O and CH_4 are absent in hot magmatic gases and assumed to be purely atmospheric in origin. The overall gas ratios with their analytical uncertainties are reported in **Table 1 in the Appendix**.

On several occasions we were able to determine the column amounts and molar ratios of SO_2, HCl and HF in the air-diluted bulk eruption plume analysing absorption spectra of the direct solar radiation passing through the plume (Francis et al., 1998). **Table 2** shows the corresponding spectral windows for their retrieval. Measurements were optimized by targeting the most transparent, ash-poor sections of the eruptive plume. To first order, the chemical ratios of these three purely volcanic gas species represent the original bulk plume emission, assuming their overall preservation during fast plume expansion and dilution (see *Section 4.3*).

4. Results

4.1. Temporal evolution of CO_2-SO_2-HCl-CO gas ratios

Fig. 2 presents the time-series of daily mean CO_2/SO_2, SO_2/HCl and CO/CO_2 molar ratios in explosive gas emissions from the summit vents, along with limited data points for degassing from the spattering and effusive flank vents. The seismic tremor amplitude (1–5 Hz) recorded at the PLPI station (Red Sísmica Canaria -RSC- of the Instituto Volcanológico de Canarias -INVOLCAN, www.involcan.org/), located about 5 km away from the vents (Llano del Pino; see **Fig. 1B**), is also shown The tremor amplitude tracks the dynamic of magma-gas flow within the upper part of the eruptive conduit, and was found to well reflect the intensity of the explosive activity (D'Auria et al., 2022).

The measured molar ratios reveal the following key observations (**Fig. 2**):

i) The CO_2/SO_2 ratio shows substantial variability, with values ranging from 2.9 to 53.2. The time-series shows an increasing trend from the beginning to the middle of the eruption, with more sustained variability towards the end. While the correlation with the volcanic tremor amplitude is less apparent in the first part of the eruption, both times series follow a similar pattern from the middle to the end of the eruptive event.

ii) The SO_2/HCl ratio generally increases during the first half of the eruption, reaching values between 5.8 and 24.6. During the second half, this ratio shows steadier oscillations, and a possible correlation with tremor amplitude is suggested by the data.

iii) The CO/CO_2 ratio remains relatively stable, ranging from 0.1×10^{-3} to 8.2×10^{-3}. Its relationship to volcanic tremor amplitude appears negligible or absent.

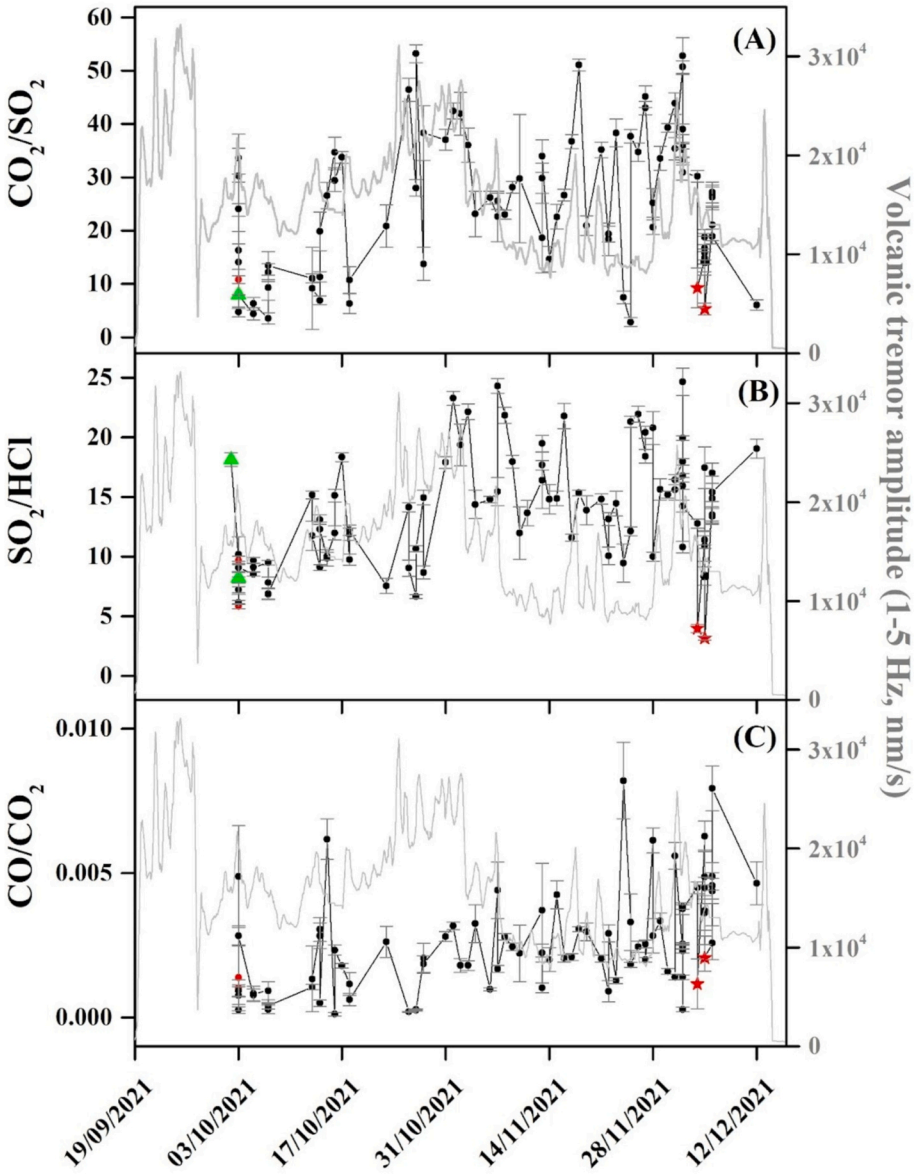

Fig. 2. Temporal variation of (A) CO_2/SO_2, (B) SO_2/HCl and (C) CO/SO_2 daily mean molar ratios in the eruptive gases from the Tajogaite summit vents, from October 3 to December 12, 2021. The grey line represents the volcanic tremor amplitude (1–5 Hz) registered at the PLPI station during the eruption. The light grey vertical lines indicate the error in the estimation of the measurements. Red solid circles correspond to measurements of the effusive degassing on October 3, 2021; the green triangles represent measurements taken from Villa José (site 3 in Fig. 1) located more than 8 km from the vents; and red stars correspond to measurements targeting a vent on lava flow on December 4 and 5, 2021.

Below, we describe in more detail our measurements during the different stages of the eruption.

On the first day of measurements (October 3), we operated two FTIR spectrometers simultaneously, one positioned at the shortest possible distance of 0.7 km (Tacande 1, site 1 in Fig. 1**C**) and the other at 2.5 km distance (Tacande 2, site 2 in Fig. 1**C**). The farthest instrument targeted the summit explosive degassing, while the closer one targeted both the summit vent and the mild-flank spattering vent. This setup allowed us to determine gas composition simultaneously emitted from each vent. The data obtained on that day are summarised in Table 3. During our observation period the intensity of explosive volcanic activity at the summit vents fluctuated significantly, oscillating between intense ash-rich emissions and more lava fountaining/intense Strombolian activity with transition periods as short as ~10 min (see Fig. 3). Notably, the magmatic CO_2 signal was so large that day that we were able to successfully detect volcanic CO_2 above the atmospheric background level from over 8 km away (site 3, Fig. 1**C**). This distance represents a record for magmatic CO_2 detection using OP-FTIR (see **Table 1 in The Appendix**).

Table 3
Summary of measurements taken on October 3, 2021.

Time UTC	*Source*	*CO_2/SO_2*	*SO_2/HCl*
14:00	Spattering vent	4.7 ± 0.9	10.2 ± 1.4
14:30	Spattering vent	10.8 ± 0.7	8.2 ± 0.5
14:21	Main ash column	16.3 ± 3.5	9.7 ± 0.3
15:12	Main ash column	14.1 ± 8.6	5.8 ± 0.2
15:39	Main ash column	24.1 ± 6.6	8.1 ± 0.3
16:15	Main ash column	33.6 ± 4.5	6.2 ± 0.2
16:25	Main ash column	30.3 ± 5.2	7.2 ± 0.3

We observed CO_2/SO_2 ratios of 4.7–10.8 for degassing at the mid-flank spattering vent. In contrast, explosive degassing from the summit vents displayed a systematically higher CO_2/SO_2 ratio that, over

Fig. 3. Activity during the measurements carried out on October 3 from Tacande 2 (site 2 in Fig. 1**C**), left at the start, right at the end.

time, increased from 16.3 to 33.6 (Table 3). A detailed analysis of our spectra, combined with simultaneous field observations demonstrates that this temporal increase was essentially determined by a wind-controlled dynamic mixing between plume emissions from the spattering vent ($CO_2/SO_2 \leq 11$) and an explosive end-member gas with CO_2/SO_2 ratio greater than 30. The proportion of this latter progressively increased as explosive activity intensified during our measurements, resulting in final CO_2/SO_2 ratios of 30.3–33.6 when only the explosive plume dominated the field of view of our spectrometer. This temporal evolution highlights the impact of viewing conditions during our OP-FTIR measurements, which depend on the wind and the position of the spectrometer with respect to the targeted vent(s). The conspicuously higher CO_2/SO_2 ratio in summit explosive degassing relative to degassing from the mild-flank spattering vent, a few hundred meters downslope, was repeatedly verified throughout the course of theeruption and, therefore, is not a measurement artefact. Rather, it indicates a preferential release of CO_2 through the main eruptive conduit controlling explosive activity at the summit of the Tajogaite cone and its spectacular depletion in secondary degassing of the magma at the mid-flank spattering vent. This rapid CO_2 depletion process is further illustrated by CO_2/SO_2 ratios as low as 2.0–0.1 for lava flow degassing at lower effusive vents recorded on the same day from in situ plume analysis with drone-based MultiGas sensors (Burton et al., 2023).

In contrast, Table 3 shows that SO_2/HCl varied little (range: 6.2–10.2) during our measurements on October 3, with no significant differences between explosive and spattering vents. Such a steadiness of SO_2/HCl ratio during otherwise distinct degassing stages of the same magma suggests a late, shallow outgassing of SO_2 together with HCl. We demonstrate below that this is consistent with the high sulfur solubility in the erupted basanitic magma controlled by its high oxidation state (see *Section 4.4*; Day et al., 2022; Burton et al., 2023).

From October 3 to October 14 data were mainly collected from Tacande 2 and Tajuya (sites 2 and 3 in Fig. 1**C**). Both sites allowed for direct measurement of degassing respectively associated with jetting of incandescent spatter at the top vents and with lava effusion from lower flank vents. During this period, explosive degassing displayed mean CO_2/SO_2 ratios ranging from 3.6 to 33.6 (average: 19.4, Fig. 2**A**), SO_2/HCl ratios from 5.8 to 15.2 (average: 9.6, Fig. 2**B**) and CO/CO_2 of (0.3–4.9)x10^{-3} (average 1.5 × 10^{-3}, Fig. 2**C**). In the following days (October 15, 16 and 17), we observed a marked increase of both CO_2/SO_2 (26.6–34.7, average 31.1) and CO/CO_2 ((0.1–6.1)x10^{-3}, average 2.6 × 10^{-3}) ratios, alongside a more gradual increase in the SO_2/HCl ratio (10.0–18.3, av. 13.1). We can hardly ascertain whether these variations were of volcanic origin or influenced by our viewing conditions and plume mixing, such as reported for our October 3 data set.

From mid-October, OP-FTIR measurements from Tajuya (site 4 in Fig. 1**C**) became increasingly challenging due to changes in the edifice's geometry, advancing lava flows, and increased ash and lapilli fallout (Fig. 4**A**). Measurements were thus taken from four new locations: Tacande 3, Dos Pinos, Las Manchas 1 and Mirador Astronómico del Llano del Jable (sites 5, 6, 7 and 8 in Fig. 1**C**). From October 17 until the morning of November 28, we recorded a trend of broad increase of both CO_2/SO_2 (average 28.3, values up to 53.2) and SO_2/HCl (6.6–24.3, average 15.3), while a relative steadiness of CO/CO_2 ((0.2–8.2)x10^{-3}, average 2.4 × 10^{-3}). It is important to note that while this increasing trend for CO_2/SO_2 and SO_2/HCl is visible in Fig. 2, some low values of the two ratios during this period can be attributed to changes in the eruptive activity or the plume direction which prevented us from capturing pure explosive emissions. Shifting wind direction was a significant factor that made our measurements more challenging during this period; on most days, two to three distinct plumes were observed, but when the wind was blowing from W-E or SW-NE the plumes tended to mix or overlap within our field of view (Fig. 4**B**).

Although the eruptive style remained broadly unchanged through early November, explosive activity at the top vents temporarily varied depending on the eruptive vent configuration. For instance, on the evening of November 6, we observed a rapid transition from ash-rich emissions to Strombolian explosions followed by lava fountaining. The gas phase driving the lava fountaining, measured from Dos Pinos (site 5 in Fig. 1), was characterized by a very high CO_2/SO_2 ratio (26.2) but also a high SO_2/HCl (14.8). This high SO_2/HCl ratio suggests that, despite intense magma fragmentation, chlorine outgassing was not significantly enhanced with respect to sulfur at that time, in contrast to what might have been expected based on previous observations of lava fountaining at Etna (La Spina et al., 2015, 2023).

Between November 25 and 27, the overall eruptive activity showed a marked decrease, with weaker lava jets at the summit and reduced lava flow rate and degassing at the effusive (front) vent. However, on

Fig. 4. (A) Picture taken November 8, 2021, showing the two FTIR spectrometers operated simultaneously. A very ashy plume can be observed. **(B)** Picture taken October 28, 2021, where the plumes overlapped with W-E wind.

November 25, an old eruptive centre reopened at the eastern end of the eruptive zone, and during the night of November 27 several vents opened in the upper NE sector of Tajogaite cone. Strombolian and effusive activity at these vents was soon replaced by a fountaining activity that developed from November 28 until December 3. During these days we were able to perform daily OP-FTIR measurements at the shortest possible distance (0.5 km) from Cabeza de Vaca (site 8 in Fig. 1C), acquiring FTIR spectra of exceptionally high quality. Fig. 5 provides an example of the results obtained from 370 spectra of lava fountaining degassing on December 2. During this stage, we recorded high values of CO_2/SO_2 and CO/CO_2 ratios (30.9–52.8, average 39.1 and (0.3–5.6)x10^{-3}, average 2.6 × 10^{-3}, respectively), while SO_2/HCl ratios remained close to the values measured during the previous weeks (10.8–24.6, average 16.7). We consider these excellent data series to be the most reliable for Tajogaite explosive degassing and, therefore, representing the bulk composition of the magmatic gas phase.

In the final two weeks of the eruption (December 3–12), the progressive decline of explosive activity allowed us close access for measuring lava jets from both sites 8 and 9 (Fig. 1C). Both were located behind and at a higher elevation than the volcanic cone, which enabled us to target the very initial path of eruptive jets inside the vents. During this period, we observed a decrease in the gas ratios: CO_2/SO_2 ranged from 6.1 to 30.2 (average 19.7), SO_2/HCl from 8.4 to 19.0 (average 13.8), and CO/CO_2 from (2.6–7.9)x10^{-3} (average 4.7 × 10^{-3}). Once again, the CO_2/SO_2 ratio varied more substantially than that of SO_2/HCl.

We highlight that on December 4, a vigorous lava flow outbreak began from an emission point located in Las Manchas 2, approximately 3 km from the summit vents (site 11 in Fig. 1C). The lava flowed at high velocities (5–10 m/s) through a lava tube system, continuing to degas vigorously at the lava tube exit. Assuming a constant flow velocity of 5–10 m/s from the summit to the effusive opening, the flow travel time

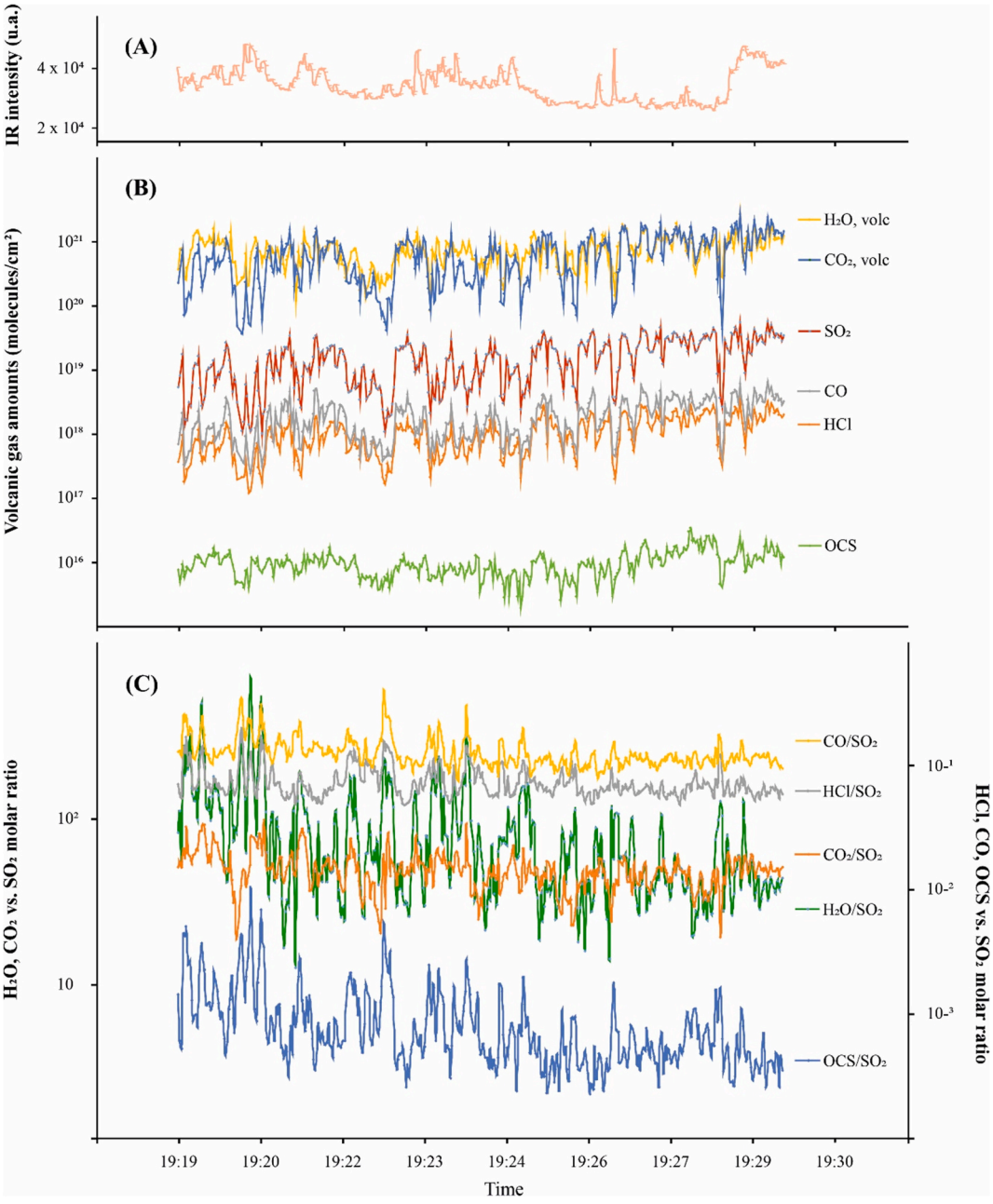

Fig. 5. Temporal variations of the (A) radiation intensity, (B) gas column amounts and (C) molar gas ratios from a best series of FTIR spectra of fire fountain degassing on December 2, 2021.

would have been 5–10 min. This rapid lava flow through the tube system likely helped to maintain high temperatures and limited outgassing until reaching the exit. We collected FTIR spectra of vigorous lava spattering at the tube exit (see red stars in Fig. 2). The results reveal CO_2/SO_2 and SO_2/HCl molar ratios of 9.3 and 4.0, respectively. We note that the CO_2/SO_2 ratio is very similar to that typical for lava spattering at the mid-flank vent of Tajogaite cone on October 3 and subsequently. When we returned to the same location one day later on December 5, the effusion intensity was significantly lower (3–5 m/s) and spattering was nearly absent. Correspondingly, the associated gas emissions showed lower CO_2/SO_2 and SO_2/HCl ratios of 5.3 and 3.2, respectively.

By mid-December 2021, all three gas ratios exhibited a rapid decline as the eruption was nearing its end, in concomitance with a net decrease in both explosive activity and seismic tremor amplitude (Fig. 2).

4.2. H_2O/SO_2 ratios and H_2O content of Tajogaite eruptive gas

Contrary to CO_2, magmatic H_2O could not be distinguished systematically from the atmospheric background. This explains why Fig. 2 does not show a temporal trend for this otherwise major component. Nevertheless, reliable quantification of magmatic H_2O was achieved on several occasions (see **Table 1 in the Appendix**). As expected, H_2O/SO_2 ratios measured on these occasions display a wide range (from 10 to >100), with a mean of 50.6 ± 43.1. However, if we consider only our series of best spectra obtained at the shortest distance from the explosive vents between late November and December 6, the H_2O/SO_2 ratio displays a much more restricted range (10.0–52.4) and an average molar ratio value of 28 (standard deviation, 13.0). For example, an average H_2O/SO_2 ratio of 31.6 was measured on December 2 (Fig. 5). The comparable molar values of CO_2/SO_2 and H_2O/SO_2 molar ratios in these best samples imply that the explosive gas phase contained about as much CO_2 as H_2O (Table 4).

4.3. SO_2-HCl-HF ratios

SO_2, HCl and HF were determined simultaneously in the bulk eruptive plume on several occasions between October 3 and December 6 using solar occultation OP-FTIR measurements (Francis et al., 1998). The measurement conditions varied, depending on the ash content of the plume and its wind-controlled expansion path, but were optimized by targeting the most transparent (ash-poor) portions of the plume. The results (see **Table 1 in the Appendix)** reveal SO_2/HCl ratios ranging from 12.2 to 24.6, comparable to those measured during explosive degassing on the same day(s). This supports our assumption of a broadly conservative behaviour of both SO_2 and HCl during plume expansion with an overall SO_2/HCl ratio averaging 18.9 (standard deviation, 6.5). At the same time HCl/HF molar ratios varied from 0.5 to 2.0, the overall average being 1.3 (standard deviation, 0.6) (Fig. 6). On October 3, during the early stage of the eruption, we measured mean SO_2/HCl and HCl/HF ratios of 22 and 1.1, respectively, for the pure explosive plume. For comparison, on November 30, towards the end of the eruption, we measured a mean plume SO_2/HCl ratio of 17.2, very close to the SO_2/HCl ratio of 15.2 directly measured in explosive emission on this same day (Table 3), and a HCl/HF ratio of 1.6. Therefore, even though we could not establish a daily database for HF, we safely consider the time-averaged HCl/HF ratio of 1.3 (standard deviation, 0.6) to be representative for explosive degassing throughout the eruptive event, as illustrated in Fig. 6.

Table 4
Initial and residual volatile abundances in the basanitic magma and mean compositions and fluxes of Tajogaite explosive and effusive gas emissions.

	CO_2	H_2O	SO_2	HCl	HF	CO
Initial magma content (wt%)	4.5 ± 1.5*	~ 3**	0.66 ± 0.12	0.075 ± 0.005	0.13 ± 0.03	n.d.
Degassed groundmass (wt%)	≤2 × 10^{-4}	0.06–0.15	0.06 ± 0.02	0.06 ± 0.01	0.095 ± 0.010	n.d.
Bulk loss rate (%)	100	97	92	17	28	n.d.
Explosive gas emission (mean)						
mol%	50.7	47.6	1.5	0.08	0.06	0.13
wt%	69.9	26.8	3.0	0.09	0.04	0.11
mass flux (kg/s)	11,500	4360	500*	15	6.3	19
*Effusive gas emission***						
mol%	10.5	87.4	1.6	0.46	n.d.	0.017
wt%	21.5	73.0	4.8	0.77	n.d.	0.023

Initial and residual abundances of H_2O, S, Cl and F were obtained from the analysis of olivine-hosted melt inclusions and the degassed groundmass of erupted products, respectively (analyses at OPGC-LMV, Clermont-Ferrand, France, and at Bristol University, UK).
n.d.: not detected.
* The original magma CO_2 content, as well as the time-averaged SO_2 flux, are from Burton et al. (2023).
** The original bulk H_2O content of 3 wt% is estimated in this study (see text, *Section 5.2*).
*** The mean composition of effusive gas emission is derived from short-distance FTIR measurement of lava flow degassing on December 4 and 5, 2021.

4.4. CO/COS/CO_2 ratios and T-redox gas state

The CO/CO_2 ratios measured for lava fountaining and explosive degassing during the whole eruption vary in the range (0.1–8.2)x10^{-3}, with an average of 2.6 × 10^{-3} (standard deviation, 0.4 × 10^{-3} (see **Table 1 in the Appendix**). The highest CO/CO_2 ratios were observed in the most reliable OP-FTIR measurements acquired between mid-November and December 6. In our series of high-quality spectra measured on December 2 (Fig. 5) we were able to additionally quantify the amount of COS coexisting with CO and CO_2. Using the molar abundances of these three carbon species (CO, CO_2 and COS) along with SO_2 from each spectrum, and combining with standard thermodynamic data (NIST Chemistry WebBook, https://webbook.nist.gov), we calculated the apparent equilibrium temperature and oxygen fugacity (fO_2) of Tajogaite magmatic gas phase at emission under atmospheric pressure from the following two redox reactions:

$$3CO + SO_2 = 2CO_2 + COS \quad (1)$$

$$CO + ½\ O_2 = CO_2 \quad (2)$$

From reaction (1), we obtain apparent gas equilibrium temperatures ranging from 957 to 1176 K (average 1087 ± 35 K). At the corresponding temperatures, the measured CO/CO_2 ratios and reaction (2)

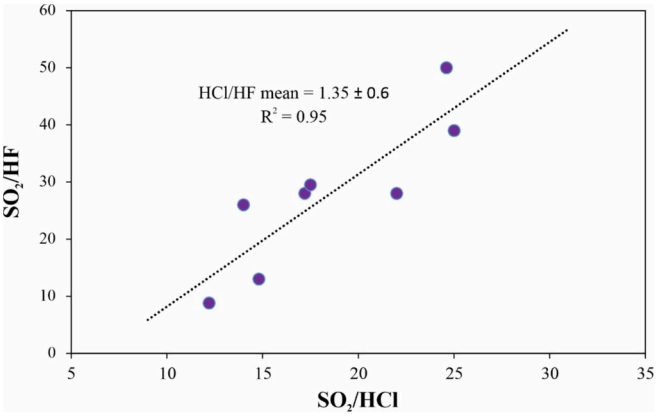

Fig. 6. SO_2-HCl-HF ratios in bulk plume emissions during Tajogaite eruption as retrieved from FTIR absorption spectra of the direct solar radiation across the plume.

yield logfO_2 values varying from −16.7 to −11.8, with an average of −13.1 ± 0.8. This points to a high oxidation state of the eruptive gas, equivalent to +1.3 ± 0.5 log unit above the Fayalite-Magnetite-Quartz (FMQ) redox buffer. This high oxidation state is consistent with the redox state of the erupted basanitic magma, ranging from FMQ +1.3 to +2.0 (average + 1.7 ± 0.3), inferred from petrological analysis of Tajogaite lavas (Day et al., 2022). Such a consistency suggests that the gas and melt were in close redox equilibrium upon emission (see *Section 5.4*). The uncertainties associated with the equilibrium temperature calculations are approximately ±35 K, derived from the variability in the best-fit temperatures for reaction (1). For oxygen fugacity (log fO_2), the uncertainty is around ±0.8 log units, reflecting the propagation of errors on the temperature determination and the measured CO/CO_2 ratios.

5. Discussion

We focus our discussion on four main aspects. We first highlight the geochemical characteristics of magmatic gases from the 2021 Tajogaite eruption in a global context by comparing them toother volcanic gases produced in analogous or different tectonic settings. Secondly, we explore the influence of magma degassing processes from depth to the surface as well as the shallow conduit geometry, on the different gas composition emitted from explosive and effusive vents, using published data for the initial content and their solubilities behaviour in the basanitic magma. Thirdly, we examine the processes responsible for the temporal variations of gas compositions during the eruption, considering seismic tremor, volcanological observations and petrological data. Finally, we discuss the redox conditions of the explosive gas emissions and their equilibrium relationship with the erupted magma.

5.1. Tajogaite magmatic gases in a global context

Tajogaite magmatic gases are compared in Fig. 7 with worldwide volcanic gases from analogous or different tectonic settings in terms of their CO_2-SO_2-HCl relative proportions. Notwithstanding the chemical

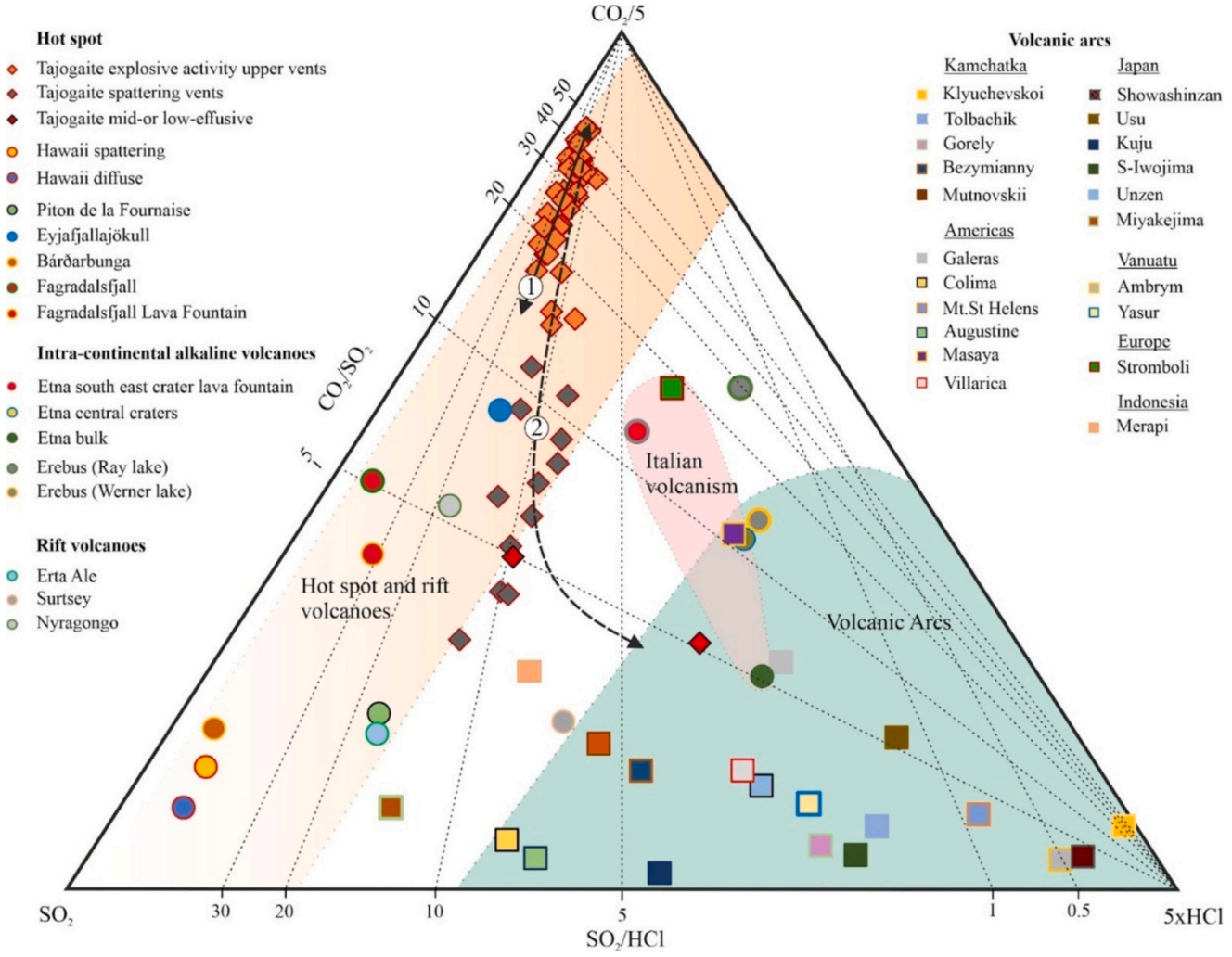

Fig. 7. The CO_2-SO_2-HCl molar composition of magmatic gases from the 2021 Tajogaite eruption, compared with the compositions of other magmatic/volcanic gases in diverse tectonic settings worldwide. Tajogaite magmatic gases typically plot within the OIB-type hot spot domain, with a low Cl content and high S/Cl ratio compared to volcanic arcs, while displaying the highest CO_2 content (CO_2/SO_2 ratio) ever observed for OIB-type magmatism. The arrow (1), through orange diamonds, delineates the temporal variations of CO_2/SO_2 ratio (from 15 to 50) at constant S/Cl ratio (around 20) for summit explosive degassing during the eruption. The curve (2), through dark grey and red diamonds, describes the simultaneous sharp CO_2-depletion (CO_2/SO_2 drop by a factor 5–10) and progressive decrease of SO_2/HCl (factor 2 to 4) during secondary then late-stage degassing at the spattering then effusive flank vents. Data extracted from Mizutani and Sugiura, 1982; Mizutani et al., 1986; Symonds et al., 1990; Giggenbach and Matsuo, 1991; Shinohara et al., 1993; Burton et al., 2000; Priatna and Kadarsetia, 2007; Burton et al., 2007; Sawyer et al., 2008; Oppenheimer and Kyle, 2008; Oppenheimer et al., 2009; Sawyer et al., 2011; Allard et al., 2011; Métrich et al., 2011; Zelenski and Taran, 2011; Shinohara, 2013; Chaplygin et al., 2015; La Spina et al., 2015; Chaplygin et al., 2016; Allard et al., 2016a; Pfeffer et al., 2018; Halldórsson et al., 2022; Scott et al., 2023; La Spina et al., 2024; Pfeffer et al., 2024.

differences between gas emissions from the upper and lower vents, linked to shallow magma degassing processes (see *Section 5.2*), we observe that Tajogaite volcanic gases typically plot within the OIB-hot spot magmatic domain. This is consistent with the OIB geochemistry of alkaline magmatism at La Palma and other Canary Islands (e.g. Hoernle et al., 1995; Lundstrom et al., 2003; Schmincke and Sumita, 2004; Day et al., 2010; Taracsák et al., 2019, 2022). The low HCl content, high SO_2/HCl ratio and very low HCl/HF ratio (1.3 ± 0.6, *Section 4.3*) of Tajogaite volcanic gases are indeed characteristic of OIB magmatism (Aiuppa et al., 2009). Moreover, their high oxidation state (*Section 4.4*), consistent with that of the erupted basanite, aligns with the oxidized nature of intra-plate alkaline magmatism in the western Canary Islands (Nicklas et al., 2022a, 2022b) and OIBs in general (e.g., Brounce et al., 2017; Moussallam et al., 2019a).

Most remarkable is the very high CO_2 content of the Tajogaite explosive gas phase. The CO_2/SO_2 molar ratios of ≥25–30, occasionally reaching ≥50, measured for lava fountaining and explosive degassing during the eruption are the highest ever recorded for any magmatic system (**Fig. 7**). Previously now, CO_2/SO_2 ratios ≥30 had been measured at very few erupting volcanoes, in particular at Mt. Etna (Allard et al., 1991; Aiuppa et al., 2007) where, however, typical CO_2/SO_2 ratios during lava fountaining events reach only ~10 (Allard et al., 2005; La Spina et al., 2015). The very high CO_2/SO_2 ratios of Tajogaite explosive gas phase cannot be attributed to a sulfur paucity in the basanitic magma which was found to contain a high and steady initial sulfur content of 0.33 ± 0.02 wt% (Burton et al., 2023). Instead, such elevated CO_2/SO_2 ratios imply a high parental CO_2 content of the basanite, assessed at 4.5 ± 1.5 wt% (Burton et al., 2023), combined with late-stage degassing of SO_2 under the oxidizing conditions of the magma (see the discussion below). A high original CO_2 content of up to 4.2 wt% was previously estimated for basanite erupted under sea water in 2011–2012 at nearby El Hierro island, based on melt inclusion data and trace element ratios (Longpré et al., 2017; Taracsák et al., 2019). A parental CO_2 content of around 4 wt% is also consistent with the Nb content of primitive melt inclusions in La Palma basanites from both 1949 and 2021 Cumbre Vieja eruptions (84–90 ppm wt; Walowski et al., 2019; Day et al., 2022) and the mean CO_2/Nb ratio typical for undergassed OIB mafic magmas (505 ± 168; Rosenthal et al., 2015). In fact, such a high CO_2 content in La Palma and El Hierro basanitic magmas is consistent with a low degree of partial melting of the HIMU-like OIB mantle source, enriched in recycled oceanic lithosphere and volatile components, that feeds the western Canary Islands (e.g., Day et al., 2010; Longpré et al., 2017; Taracsák et al., 2019; Walowski et al., 2019; Day et al., 2022). This implies a quite unique genesis of CO_2-rich mantle melts beneath the Canary Islands and highlights that CO_2 emissions produced during the formation of the whole archipelago may have been prodigious (Burton et al., 2023).

5.2. Controls on gas compositions from magma degassing processes and the conduit system geometry

The composition of Tajogaite magmatic gases, along with the sharp chemical contrast between gas emissions from explosive and effusive degassing during the eruption, offer insight into the magma degassing processes from depth to the surface and the geometry of the shallow conduit system.

Seismic data (D'Auria et al., 2022) showed the involvement of two distinct magma storage zones before and during the eruption: one located at 10–16 km depth (around the Moho interface) and a deeper one at 27–31 km depth in the mantle. The initially erupted magma, an olivine-poor evolved basanite (Pankhurst et al., 2022; Day et al., 2022), rapidly ascended from the shallow magma storage level, of 10 km to the surface in 7 days (D'Auria et al., 2022), i.e. at an average rate of 60 m per hour. Since early October 2021, when we started our OP-FTIR measurements, this magma was gradually replaced by a more primitive olivine-rich basanite from the deeper reservoir, as suggested by petrological data (Day et al., 2022; Burton et al., 2023; Zanon et al., 2024) and by the intense seismicity (M > 3 and up to 4.3) that began to develop at that depth (D'Auria et al., 2022). Both seismogenic domains remained active until the end of the eruption (D'Auria et al., 2022).

Interestingly, olivine crystals in Tajogaite lavas and tephra erupted since early October 2021 ubiquitously contained CO_2-rich fluid inclusions that exhibited a bimodal density distribution perfectly matching the depth ranges of the two seismogenic magma storage zones (Zanon et al., 2024). This observation thus implies that an exsolved CO_2-rich gas phase already coexisted with the magma at mantle depths of 27–31 km and at the shallower storage zone (10–16 km depth). Basanitic melt inclusions entrapped in olivine crystals at ~10–12 km depth (290 to ~350 MPa pressure) contained dissolved amounts of 0.22–0.50 wt% CO_2 and 1.30–2.21 wt% H_2O (Burton et al., 2023), in addition to 0.33 ± 0.06 wt% S, 0.07 ± 0.01 wt% Cl and 0.13 ± 0.03 wt% F (**Table 4**). Therefore, at those depths about 89 % (~4 wt%) of the parental CO_2 content of the basanitic magma (4.5 ± 1.5 wt%; Burton et al., 2023) had already exsolved. According to solubility data for H_2O and CO_2 in La Palma basanite (Jimenez-Mejias et al., 2021), this CO_2 may have coexisted with ~1 wt% exsolved H_2O, which, when added to the dissolved H_2O amount in melt inclusions at ~10–12 km depth, implies a total H_2O content of 2.3–3.2 wt% in the magmatic system (**Table 4**). The nearly constant S content in the melt inclusions (Burton et al., 2023) and the absence of any S species in the fluid inclusions (Zanon et al., 2024) indicate no sulfur exsolution at that level. Therefore, on a molar basis, the fluid phase exsolved at 10–12 km depth consisted of 62 mol% CO_2 and 38 mol% H_2O. While we do not exclude the possibility of a pre-eruptive accumulation of deeper-derived pure CO_2 at this level, the gradual emptying of a CO_2-enriched reservoir is expected to generate highest CO_2/SO_2 and CO_2/HCl ratios at the beginning of the eruption, followed by a temporal decrease of these ratios as the eruption progresses. The absence of such a trend in our dataset – where CO_2/SO_2 ratios tended to increase during the first half of the eruption or remained elevated during most of the event (see **Fig. 2**) – suggests that pre-eruptive CO_2 accumulation at depth was minimal.

Rapid magma ascent from ≥10 km depth, as indicated by seismic data (D'Auria et al., 2022), likely favoured closed system decompression and exsolution of magmatic volatiles, thus limiting the extent of gas-magma separation until near the surface. The average molar composition of Tajogaite explosive gas phase during the eruption (50.7 mol% CO_2, 47.6 mol% H_2O, 1.5 mol% SO_2, 0.08 mol% HCl, 0.06 mol% HF and 0.13 mol% CO; **Table 4**) is consistent with the closed system ascent of the magma-gas mixture to shallow depth. This is based on the initial volatile abundances described above and the modelled solubility behaviour of CO_2, H_2O and SO_2 in the decompressing basanite (Burton et al., 2023).The low SO_2 content along with the high CO_2/SO_2 and H_2O/SO_2 ratios of the explosive gas phase can be attributed to the high oxidation state of the erupting basanite (Day et al., 2022), which enhanced sulfur solubility and led to shallow SO_2 exsolution and outgassing (Burton et al., 2023).

However, the sharp contrasts in CO_2/SO_2 and CO_2/HCl ratios, and to a lesser extent in SO_2/HCl ratio, between explosive degassing at the upper vents and spattering-effusive degassing at the lower flank vents (**Fig. 7**) indicate that volatile fractionation through open system degassing occurred above some shallow point in the feeding dyke. Such a chemical contrast during degassing of the same magma, persisting at vents only a few hundred meters apart during an entire eruption, implies a gas fractionation pattern controlled by the geometry of the shallow conduit system. We envision a shallow branching beneath Tajogaite cone where a sub-vertical conduit favoured the explosive release of the CO_2-rich gas phase through the upper vents, while a tilted branch drained most of the magma and the remaining CO_2-depleted gas towards the lower flank effusive vents (**Fig. 8**). In fact, during the whole eruption 76 % of the total magma volume was outpoured as lava flows from the flank vents, while only 24 % was emitted as tephra and ash from the summit craters (Bonadonna et al., 2022; Burton et al., 2023). Gas-

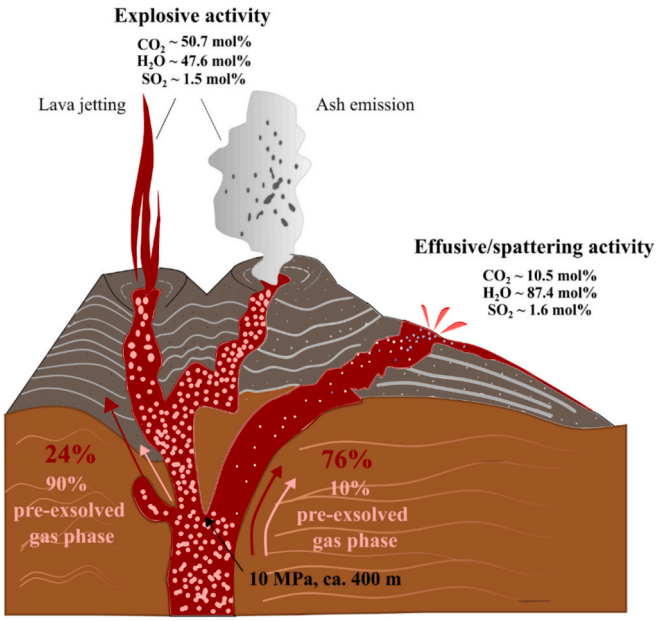

Fig. 8. Schematic representation of the shallow conduit branching, which controlled the compositional gas contrasts during simultaneous explosive and effusive eruptive activity of the 2021 Tajogaite event. A depth of ~400 m (10 MPa) is estimated for the conduit branch point where gas-magma partitioning occurred. Indicated are the time-averaged proportions of the pre-exsolved gas phase at the branching point, as well as the bulk magma supply that respectively fed the summit vents and the lateral (flank) vents of the Tajogaite volcanic cone. Also shown are the measured mean weight proportions of CO_2, H_2O and SO_2 in the summit explosive gas emissions and the flank effusive emissions.

magma separation at a shallow conduit branching point is of common occurrence at basaltic volcanoes that simultaneously erupt both explosively and effusively (e.g., Burton et al., 2003; La Spina et al., 2010). This magmatic partitioning results in a different chemical composition and mass flux of the exsolved gas phase in each conduit branch, depending on the depth of the branch point, the solubility dynamics of each volatile species in the melt, and the gas/magma flow ratio in each branch. The flux of volatiles at the surface represents the sum of exsolved gases in each branch, along with any contribution from volatiles dissolved in melt at the branch point.

Based on the relative altitude (250 m) and distance (300 m) between the explosive summit vents and the spattering-effusive flank vents of the Tajogaite volcanic cone, we estimate a maximum depth of 400 m for the branching point. At the corresponding pressure of ca. 10 MPa and under the T-redox conditions of the magma (Day et al., 2022), C-H-O-S solubility modelling for closed-system ascent of basanitic-type magma (Moretti et al., 2003) with the initial volatile contents described above indicates that, at the branching point, CO_2 is entirely degassed (20 wt ppm left in the melt), while ≤1 wt% H_2O and ~ 90 % of total sulfur (2700 wt ppm) still remain dissolved in the melt. Most of the pre-exsolved gas phase at this level is expected to rise preferentially in the sub-vertical summit branch (**Fig. 8**) together with a modest proportion of the bulk erupted magma (Bonadonna et al., 2022; Burton et al., 2023). **Fig. 9** shows the expected variations of CO_2/SO_2 and H_2O/SO_2 ratios in the summit gas emissions as a function of the percentage of co-supplied magma, assuming that 90 wt% of the pre-exsolved gas phase rises through the summit branch. The best representative range of CO_2/SO_2 and H_2O/SO_2 ratios measured in the Tajogaite explosive gas, 20–50, suggests the co-involvement of between only 10 % and 30 wt% of the total ascending magma in the vertical transport to the summit vents, the remainder being erupted through the effusive flank vents. Consequently, the magmatic mixture entering the summit branch and erupting from the summit vents likely had a very high volatile mass fraction. This

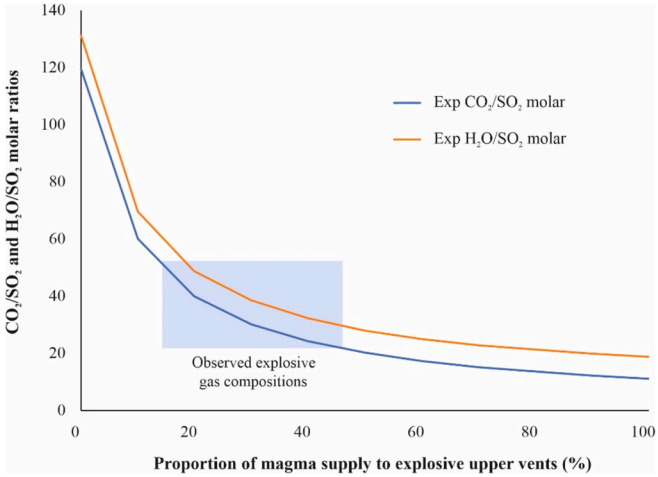

Fig. 9. Calculated variations of CO_2/SO_2 and H_2O/SO_2 ratios in Tajogaite explosive emissions as a function of the percentage of bulk ascending magma co-supplied to the summit vents. These calculations assumed that 90 wt% of the exsolved gas phase at the branchng point, containing all the initial CO_2 (4.5 wt %), 2/3rd of the initial H_2O content (3 wt%) and only 10 wt% of the available magma sulfur content (0.27 wt%), was rising towards the summit vents. The measured best range of CO_2/SO_2 and H_2O/SO_2 ratios in Tajogaite's explosive gas, 20–50, indicates that 10 wt% and 30 wt% of the total ascending magma was involved in the summit eruption, with the remainder being erupted at the effusive vents. These proportions agree with independent estimates of the respective mass eruption rates (Bonadonna et al., 2022; Burton et al., 2023).

volatile mass fraction can be estimated by comparing the gas emission rate to the time-averaged magma eruption rate from the summit vents (2×10^4 kg/s; Burton et al., 2023). Using the time-averaged SO_2 flux of 500 ± 200 kg/s constrained from TROPOMI satellite data (Burton et al., 2023) and the mean weight composition of the explosive gas phase (**Table 4**), we calculate the mass flux of each volatile component and a total gas emission rate of 1.6×10^4 kg/s (**Table 4**). This yields a mean gas mass fraction of 0.45. Such a high value well accounts for the high explosivity of the magmatic mixture, the high level of magma fragmentation, and the rapid transitions in eruption style as varying amounts of magma entered the summit branch.

Finally, it is known that chlorine and fluorine rarely reach saturation during the eruption of mafic magmas and tend to partition into the co-existing fluid phase at relatively shallow depths (e.g. Carrol and Webster, 1994; Alletti et al., 2009; Baker and Alletti, 2012). Here we assess the fluid-melt partition coefficient for Cl and F during the eruption of Tajogaite basanite by analysing their respective concentrations in the explosive gas phase and in the melt, assuming gas-melt equilibrium. The Cl and F concentrations in the melt were estimated from their average concentrations in the groundmass glass of the erupted products (0.06 ± 0.01 wt% and 0.095 ± 0.010 wt%, respectively). Using the mass concentrations of Cl (0.09 wt%) and F (0.04 wt%) in the explosive gas (**Table 4**), we calculate fluid-melt partition coefficients of 1.5 and 0.4 for Cl and F, respectively. The low partition coefficient for Cl in the case of Tajogaite basanite is consistent with experimental observations showing an increased affinity of Cl for the melt in CO_2-rich mafic magmas (Alletti et al., 2009).

5.3. *Temporal evolution of gas emissions during the eruption*

Comparison of the time series for the gas composition and tremor during the eruption, as shown in **Fig. 2**, is illuminating. CO_2/SO_2 ratios increased with both increasing explosivity and increasing tremor, which we interpret in terms of a relative reduction in the proportion of magma supplied to the summit conduit. This led to an increased gas/magma ratio, deeper magma fragmentation and greater explosive velocities,

albeit with a lower overall magma eruption rate. This is consistent with the rapid transition between eruption styles – from fire fountains to ash-rich venting, and Strombolian activity – where higher gas/magma ratios favoured fragmentation and ash-rich plumes whereas lower gas/magma ratios favoured Strombolian activity.

To interpret the observed variations of gas composition during the eruption (**Fig. 2**) we consider the influence of both shallow and deep processes. During the first week of our measurements (October 3–7, 2021), as the Tajogaite edifice was still in its early growth stage, the upper magma interface was likely closer to the surface and the effusive/explosive vents were less distant. As a result, most of the lava flows came out near the top of the principal conduit. This likely promoted SO_2 and HCl outgassing through this conduit, resulting in the observed minor difference in SO_2/HCl ratio between explosive and effusive degassing during this period (see *Section 4.1*). During this interval, we actually observed moderately high CO_2/SO_2 and SO_2/HCl ratios in gas emissions from the summit vents (*Section 4.1* and **Fig. 2**), even though a very high CO_2/SO_2 of 53 had been measured on October 3 using in situ MultiGas plume analysis (Burton et al., 2023).

As the eruption progressed, the volcanic edifice grew both in volume and height, resulting in a relative deepening of the branching point and increasing the distance between the upper and the flank vents. Consequently, this provided a greater opportunity for gas differentiation at the distinct vents, which may partly explain the increase in the CO_2/SO_2 and SO_2/HCl ratios during October 13–17 (**Figs. 2A, B**). However, we do not exclude the possibility that improved visibility of the pure explosive gas phase during this period contributed to the observed changes. Another possible explanation is the increasing supply of more primitive basanite, richer in olivine, with a lower Sr isotope ratio and more anorthite-richer plagioclase microlites in its groundmass (Ubide et al., 2023), that was rising from the deeper (20–27 km) seismogenic reservoir (Day et al., 2022; Zanon et al., 2024). From October 17 to 23, both CO_2/SO_2 and SO_2/HCl ratios sharply decreased (respectively from 33.7 to 6.3 and from 18.3 to 7.6), despite increasing tremor and explosive activity. We consider this drip in the gas ratios as likely due to degraded viewing conditions or/and a high ash content in summit emissions during that period. In fact, CO_2/SO_2 rapidly increased again afterward, reaching very high values by the end of October, while SO_2/HCl persisted at low to moderate values until October 31. Such a trend, associated with increasing amplitude of the volcanic tremor (**Fig. 2**), is compatible with a greater proportion of magma and gas reaching the surface through the main explosive conduit, leading to enhanced magma fragmentation (Gonnermann and Taisne, 2015)and more effective Cl release (La Spina et al., 2015), thereby maintaining low to moderate SO_2/HCl ratios for several days while CO_2 was increasingly abundant in summit degassing.

From early to mid-November, both the tremor and CO_2/SO_2 ratio tended to decrease, whereas SO_2/HCl displayed high values (**Fig. 2**). This is consistent with a lower magma ascent rate (Zanon et al., 2024) and lower magma fragmentation at the surface, as well as with petro-geochemical evidence for the contemporaneous involvement of two distinct magma batches during this period. These batches originated from the two different storage depths, which are characterized by different Sr (Ubide et al., 2023) and Os (Day et al., 2022) isotope ratios. Following this period, both CO_2/SO_2 and SO_2/HCl ratios recovered to very high values, with short-term oscillations, until the first week of December. On November 24 we measured both low CO_2/SO_2 and SO_2/HCl ratios, indicating a possible change in the geometry of the eruptive conduit, possibly associated with a partial collapse of the cone, which may have affected the magma-gas distribution. This abrupt variation coincided with a lower activity at the top vents and with a significantly reduced lava emission rate at the low flank vents. As described in *Section 4.1*, this sharp but brief reduction in summit activity was followed by a sudden reactivation of one of the back-top vents on November 25 then the opening of two new NW eruptive vents, which produced vigorous lava fountaining and lava flows between November 27 and December 3. These changes in surface activity are reflected in the variations of both seismic tremor and gas chemistry (**Fig. 2**). During this period, we recorded among the highest CO_2/SO_2 ratios (52.8) of the entire eruption. According to Zanon et al. (2024), at that time the magma was uprising from great depth at a high mean velocity of 0.03 m/s, without any ponding in the shallower intermediate storage zone. Starting from December 1, the deep seismic activity rapidly declined, marking the termination of magma supply from mantle depths, while the intermediate seismic activity gradually decreased. This final stage of the eruption, characterized by a marked decrease in the anorthite content of plagioclase microlites in the matrix glass of erupted lavas (Ubide et al., 2023) is well reflected in the synchronous sharp decline of CO_2/SO_2, SO_2/HCl and CO/SO_2 ratios in summit gas emissions (**Fig. 2**).

5.4. Gas-magma redox equilibrium

High-temperature volcanic gases co-erupting with their host magma are generally found to be in thermodynamic equilibrium with this magma (e.g., Gerlach and Nordie, 1975; Allard et al., 1977; Giggenbach, 1996). However, recent studies suggest that this equilibrium may be disrupted during rapid gas ascent and cooling. For example, Oppenheimer et al. (2018) found that the composition of volcanic gas emitted from the Halema'uma'u lava lake of Kīlauea in 2015 was consistent with a closed-system equilibrium driven by rapid adiabatic cooling in ascending gas slugs. Similarly, Moussallam et al. (2019b) argued that explosive activities can cause deviation from gas-magma redox equilibrium due to the rapid adiabatic expansion of the gas phase.

As shown in *Section 4.4*, our results for the Tajogaite eruption indicate that the explosive gas phase maintained a redox state of FMQ +1.3 ± 0.5 at 1087 ± 35 K on average, very close to that of the erupted basanite throughout the eruption (FMQ +1.7 ± 0.2; Day et al., 2022). In fact, our calculated value falls within the error range of the average value reported by Day et al. (2022). Such a consistency supports the preservation of gas-magma redox equilibrium upon emission, even as the gases underwent rapid cooling and air dilution.

Fig. 10 illustrates the fO_2-T dynamic range of the explosive gas phase on December 2 (red curve) (see *Section 4.1* and **Fig. 5**). The observed gas variation pattern parallels the FMQ +1.7 ± 0.2 (Day et al., 2022) redox state inferred for the magma (orange curve), suggesting redox buffering of the gas phase by the co-erupted tephra. This observation highlights that, in the case of Tajogaite explosive activity, gas-magma redox buffering was dominating over potential disequilibrium effects caused by adiabatic gas expansion.

Finally, we highlight that even the lowest apparent equilibrium temperature of 957 K computed for explosive degassing (*Section 4.4*) is much higher than the physical gas temperature of approximately 400 K inferred from SO_2 absorption bands in our FTIR spectra (*Section 3*). This also applies to degassing from the spattering and effusive flank vents, where CO/CO_2 ratios indicate apparent equilibrium temperatures ranging from 700 to 1340 K (average 980 ± 300 K). Therefore, our study further demonstrates that the kinetics of chemical re-equilibration or/and oxidation of eruptive volcanic gases upon emission is much slower than their actual physical cooling through expansion and air dilution (e.g., Giggenbach, 1996; Allard et al., 2005).

6. Conclusions

We present the very first detailed data set on the chemical composition of magmatic gases emitted during a subaerial eruption in the Canary archipelago, providing new insights into the volatile geochemistry of OIB-type alkaline magmatism in this region.

Our daily OP-FTIR measurements of gas emissions during the 85-days long 2021 Tajogaite eruption of Cumbre *V*ieja volcano on La Palma Island, provide the most comprehensive data set ever obtained for the chemical evolution of magma degassing during a volcanic eruption. Our measurements during this 85-day long eruptive event document the compositional features and temporal changes of gas emissions generated

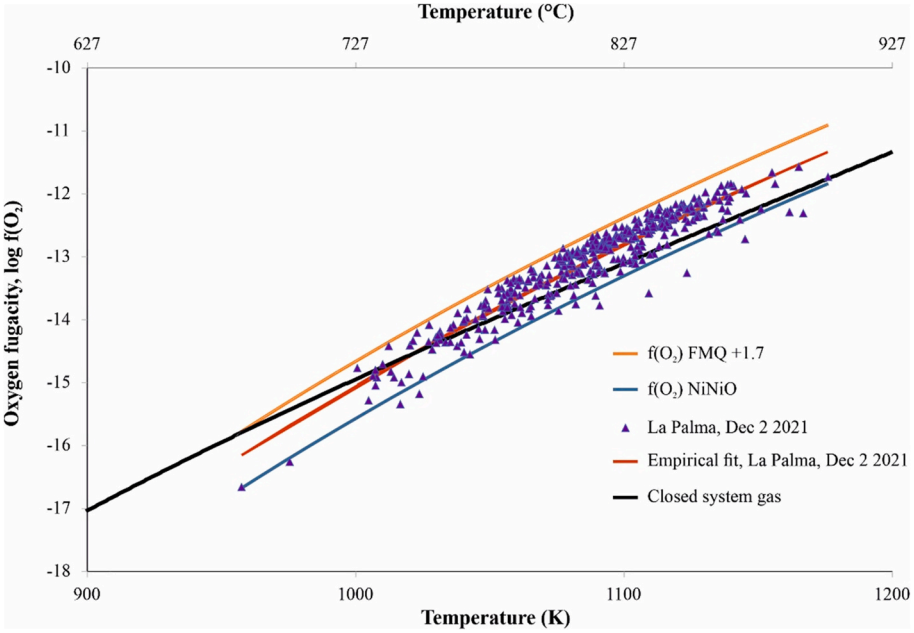

Fig. 10. fO_2 temperature variation pattern of Tajogaite explosive gas (orange curve, QFM +1.3 ± 0.5), as derived from the molar proportions of CO_2, SO_2, CO and COS in our best FTIR spectra collected on 2 December 2021 (see text). Also shown are the NNO (Nickel-Nickel Oxide) redox buffer and the mean FMQ + 1.7 ± 0.2 redox state (red curve) inferred for the erupted basanitic magma (Day et al., 2022). The black curve depicts the modelled fO_2-T evolution for closed-system compositional re-equilibration of the gas phase upon cooling. Data points discard this latter process indicating predominant redox buffering of the gas phase by the co-erupted pyroclasts.

by magmatic processes associated with both explosive and effusive activity. We note that our early data for explosive degassing, before approximately October 20, were more affected by mixing with plume gases coming from the spattering vent than subsequent measurements, which may account for the general observation of lower CO_2/SO_2 ratios before that date and the apparent trend of increasing ratio over time. As the morphology of the Tajogaite volcanic cone evolved favourably, it became easier for us to measure pure gas emissions from the fountaining and explosive activities at the upper vents. This allowed us to retrieve the same high CO_2/SO_2 ratios as measured on October 3 and afterward. Similarly, the SO_2/HCl data show that the effusive vents emitted higher concentrations of SO_2 and HCl than explosive emissions from the summit vents, with lower SO_2/HCl ratio reflecting enhanced Cl release.

Once the bearing of secondary influences is minimized, our OP-FTIR dataset documents significant changes in gas composition over the course of the Tajogaite eruption, driven by the dynamical evolution of gas and magma flows in an evolving plumbing system. Especially, the persistence of a distinct CO_2-rich signature of explosive emissions from the upper vents compared to effusive degassing from lower flank vents implies a sharp transition from closed system to open system magma degassing at a shallow branching point beneath the growing Tajogaite volcanic cone. We show that explosive activity at the summit vents was supplied by the partitioning of CO_2-rich gas and relatively modest amounts of magma in a main vertical conduit, with temporal variations in the gas-magma ratio determining rapid transitions in eruptive style. Instead, a tiny fraction of the early exsolved CO_2-rich gas phase and most of the magma were drained out through tilted conduit branches feeding the effusive vents. Late-stage shallow degassing of SO_2 was a specific feature of the 2021 Cumbre Vieja eruption, linked to the high oxidation state of the erupted basanitic magma. In addition to a high original CO_2 content of the magma (Burton et al., 2023), this explains the low SO_2 content and very high CO_2/SO_2 ratio of explosive emissions from the summit vents, increasingly obvious as the growing height of Tajogaite cone increased the confining pressure of the branching point. This configuration favoured late-stage SO_2 degassing during lava spattering and lava flow outpouring at lower flank vents.

Finally, our study reveals a relatively close correlation between CO_2/SO_2 ratio and volcanic tremor during the evolution of explosive activity at the summit vents of a volcanic cone, suggesting that tremor amplitude was intimately determined by the gas (CO_2) content of magmatic flow through the main eruptive conduit. Our results thus provide further insights into the complex dynamics of mixed explosive-effusive eruptions and further demonstrate the remarkable potential of OP-FTIR spectroscopy for detailed investigation of magma degassing processes during volcanic eruptions in general.

Funding

This research was financially supported by the projects VOLRISK-MAC II (MAC2/3.5b/328), financed by the INTERREG V-A Spain-Portugal MAC 2014–2020 Territorial Cooperation Program of the European Commission; Cumbre Vieja Emergencia, financed by the Science and Innovation Ministry, Spanish Government; and TFassistance, financed by the Cabildo Insular de Tenerife and Instituto Tecnológico y de Energías Renovables. This work was also supported by UKRI NERC project V-PLUS NE/S004106/1 and COMET, www.comet.nerc.ac.uk.

CRediT authorship contribution statement

María Asensio-Ramos: Visualization, Validation, Resources, Project administration, Methodology, Investigation, Formal analysis, Data curation, Conceptualization, Writing – review & editing, Writing – original draft. **Ana Pardo Cofrades:** Visualization, Validation, Resources, Project administration, Methodology, Investigation, Formal analysis, Data curation, Conceptualization, Writing – review & editing, Writing – original draft. **Mike Burton:** Visualization, Validation, Supervision, Software, Resources, Project administration, Methodology, Investigation, Funding acquisition, Formal analysis, Data curation, Conceptualization, Writing – review & editing, Writing – original draft. **Alessandro La Spina:** Visualization, Validation, Supervision, Resources, Methodology, Investigation, Formal analysis, Data curation, Conceptualization, Writing – review & editing, Writing – original draft.

Patrick Allard: Visualization, Validation, Supervision, Methodology, Investigation, Formal analysis, Data curation, Conceptualization, Writing – review & editing, Writing – original draft. **José Barrancos:** Resources, Methodology, Investigation, Data curation. **Catherine Hayer:** Software. **Ben Esse:** Software. **Luca D'Auria:** Software, Resources, Project administration, Investigation, Funding acquisition, Data curation. **Pedro A. Hernández:** Resources. **Eleazar Padrón:** Resources. **Gladys V. Melián:** Resources. **Nemesio M. Pérez:** Supervision, Resources, Project administration, Funding acquisition, Conceptualization.

Declaration of competing interest

The authors declare that they have no known competing financial interests or personal relationships that could have appeared to influence the work reported in this paper.

Data availability

Data is provided in the manuscript (Table 1 in Appendix)

Acknowledgements

Complementary support was provided by Istituto Nazionale di Geofisica e Vulcanologia (INGV, Italy), Institut de Physique du Globe de Paris (France) and the International Association of Volcanology and Chemistry of the Earth Interior (IAVCEI). We are also very grateful to Antonio Álvarez for his assistance during fieldwork and William Hernández-Ramos for his contribution to Fig. 2.

Appendix A. Supplementary data

Supplementary data to this article can be found online at https://doi.org/10.1016/j.chemgeo.2024.122605.

References

Aiuppa, A., Federico, C., Paonita, A., Pecoraino, G., Valenza, M., 2002. S, Cl and F degassing as an indicator of volcanic dynamics: the 2001 eruption of Mount Etna. Geophys. Res. Lett. 29. https://doi.org/10.1029/2002GL015032, 54-1-54–4.

Aiuppa, A., Moretti, R., Federico, C., Giudice, G., Gurrieri, S., Liuzzo, M., Papale, P., Shinohara, H., Valenza, M., 2007. Forecasting Etna eruption by real time evaluation of volcanic gas composition. Geology 35, 1115–1118. https://doi.org/10.1130/G24149A.

Aiuppa, A., Baker, D., Webster, J., 2009. Halogens in volcanic systems. Chem. Geol. https://doi.org/10.1016/j.chemgeo.2008.10.005.

Allard, P., Le Guern, F., Sabroux, J.C., 1977. Thermodynamic and isotopic studies of eruptive gases. Geothermics 5, 37–40. https://doi.org/10.1016/0375-6505(77)90006-2.

Allard, P., Carbonnelle, J., Dajlevic, D., Le Bronec, J., Morel, P., Maurenas, J.M., Robe, M.C., Faivre-Pierret, R., Sabroux, J.C., Zettwoog, P., 1991. Eruptive and diffuse emissions of carbon dioxide from Etna volcano. Nature 351, 387–391. https://doi.org/10.1038/351387a0.

Allard, P., Burton, M., Mure, F., 2005. Spectroscopic evidence for a lava fountain driven by previously accumulated magmatic gas. Nature 433 (7024), 407–410. https://doi.org/10.1038/nature03246.

Allard, P., Burton, M., Oskarsson, N., Michel, A., Polacci, M., 2010. Chemistry and fluxes of magmatic gases driving the explosive trachyandesitic phase of Eyjafjallajökull 2010 eruption: constraints on degassing magma volumes and processes. In: AGU Fall Meeting, San Francisco, December 2010, V53F-07.

Allard, P., La Spina, A., Tamburello, G., Aiuppa, A., Coquet, A., Brenguier, F., Coppola, D., Di Muro, A., Burton, M., Staudacher, T., 2011. First Cross-Correlated Measurements of Magma Dynamics and Degassing during a Dyke Eruption at Piton de la Fournaise Hot Spot Volcano, Réunion Island. AGU Fall Meeting, San Francisco, V22A-04.

Allard, P., Aiuppa, A., Bani, P., Métrich, N., Bertagnini, A., Gauthier, P.-J., Shinohara, H., Sawyer, G., Parello, F., Bagnato, E., Pelletier, B., Garaebiti, E., 2016a. Prodigious emission rates and magma degassing budget of major, trace and radioactive volatile species from Ambrym basaltic volcano, Vanuatu island Arc. J. Volcanol. Geotherm. Res. 322, 119–143. https://doi.org/10.1016/j.jvolgeores.2015.10.004.

Allard, P., Burton, M., Sawyer, G., Bani, P., 2016b. Degassing dynamics of basaltic lava lake at a top-ranking volatile emitter: Ambrym volcano, Vanuatu arc. Earth Planet. Sci. Lett. 448, 69–80. https://doi.org/10.1016/j.epsl.2016.05.014.

Alletti, M., Baker, D.R., Scaillet, B., Aiuppa, A., Moretti, R., Ottolini, L., 2009. Chlorine partitioning between a basaltic melt and H_2O–CO_2 fluids at Mount Etna. Chem. Geol. 263, 37–50. https://doi.org/10.1016/j.chemgeo.2009.04.003.

Amonte, C., Melián, G.V., Asensio-Ramos, M., Pérez, N.M., Padrón, E., Hernández, P.A., D'Auria, L., 2023. Hydrogeochemical temporal variations related to the recent volcanic eruption at the Cumbre Vieja Volcano, La Palma, Canary Islands. Front. Earth Sci. 10. https://doi.org/10.3389/feart.2022.1003890, 1003890.

Ancochea, E., Hernán, F., Cendrero, A., Cantagrel, J.M., Fúster, J., Ibarrola, E., Coello, J., 1994. Constructive and destructive episodes in the building of a young Oceanic Island, La Palma, Canary Islands, and genesis of the Caldera de Taburiente. J. Volcanol. Geotherm. Res. 60, 243–262. https://doi.org/10.1016/0377-0273(94)90054-X.

Baker, D.R., Alletti, M., 2012. Fluid saturation and volatile partitioning between melts and hydrous fluids in crustal magmatic systems: the contribution of experimental measurements and solubility models. Earth Sci. Rev. 114, 298–324. https://doi.org/10.1016/j.earscirev.2012.06.005.

Baker, D.R., Moretti, R., 2011. Modeling the solubility of sulfur in magmas: A 50-year old geochemical challenge. In: Behrens, H., Webster, J.D. (Eds.), Sulfur in Magmas and Melts: Its Importance for Natural and Technical Processes: Rev. Mineral. Geochem, vol. 73, pp. 167–213. https://doi.org/10.2138/rmg.2011.73.7.

Bamber, E.C., la Spina, G., Arzilli, F., Polacci, M., Mancini, L., de' Michieli Vitturi, M., Andronico, D., Corsaro, R. A., Burton, M. R., 2024. Outgassing behaviour during highly explosive basaltic eruptions. Commun. Earth Environ. 5, 3. https://doi.org/10.1038/s43247-023-01182-w.

Blank, J.G., Brooker, R.A., 2018. Experimental studies of carbon dioxide in silicate melts: solubility, speciation, and stable carbon isotope behavior. In: Volatiles in Magmas, 30, pp. 157–186. https://doi.org/10.1515/9781501509674-011.

Blundy, J., Mavrogenes, J., Tattitch, B., Sparks, S., Gilmer, A., 2015. Generation of porphyry copper deposits by gas–brine reaction in volcanic arcs. Nat. Geosci. 8, 235–240. https://doi.org/10.1038/ngeo2351.

Bonadonna, C., Pistolesi, M., Biass, S., Voloschina, M., Romero, J., Coppola, D., Folch, A., D'Auria, L., Martin-Lorenzo, A., Dominguez, L., Pastore, C., Reyes Hardy, M.P., Rodríguez, F., 2022. Physical characterization of long-lasting hybrid eruptions: the 2021 Tajogaite Eruption of Cumbre Vieja (La Palma, Canary Islands). J. Geophys. Res. Solid Earth 127 (11). https://doi.org/10.1029/2022JB025302.

Brounce, M., Stolper, E., Eiler, J., 2017. Redox variations in Mauna Kea lavas, the oxygen fugacity of the Hawaiian plume, and the role of volcanic gases in Earth's oxygenation. Proc. Natl. Acad. Sci. 114, 8997–9002. https://doi.org/10.1073/pnas.1619527114.

Burton, M., Oppenheimer, C., Horrocks, L.A., Francis, P.W., 2000. Remote sensing of CO_2 and H_2O emission rates from Masaya Volcano, Nicaragua. Geology 28, 915–918. https://doi.org/10.1130/0091-7613(2000)028<0915:rsocah>2.3.co;2.

Burton, M., Allard, P., Murè, F., Oppenheimer, C., 2003. FTIR remote sensing of fractional magma degassing at Mount Etna, Sicily. Geol. Soc. Spec. Publ. 213, 281–293. https://doi.org/10.1144/GSL.SP.2003.213.01.17.

Burton, M., Allard, P., Mure, F., La Spina, A., 2007. Magmatic gas composition reveals the source depth of slug-driven strombolian explosive activity. Science 317, 227–230. https://doi.org/10.1126/science.1141900.

Burton, M., Aiuppa, A., Allard, P., Asensio-Ramos, M., Cofrades, A.P., la Spina, A., Nicholson, E.J., Zanon, V., Barrancos, J., Bitetto, M., Hartley, M., Romero, J.E., Waters, E., Stewart, A., Hernández, P.A., Lages, J.P., Padrón, E., Wood, K., Esse, B., Hayer, C., Cyrzan, K., Rose-Koga, E.F., Schiavi, F., D'Auria, L., Pérez, N.M., 2023. Exceptional eruptive CO_2 emissions from intra-plate alkaline magmatism in the Canary volcanic archipelago. Nat. Commun. Earth Environ. 4, 467. https://doi.org/10.1038/s43247-023-01103-x.

Carracedo, J.C., Day, S.J., Guillou, H., Gravestock, P., 1999. Later stages of volcanic evolution of La Palma, Canary Islands: Rift evolution, giant landslides, and the genesis of the Caldera de Taburiente. Bull. Geol. Soc. Am. 111, 755–768. https://doi.org/10.1130/0016-7606(1999)111<0755:LSOVEO>2.3.CO;2.

Carracedo, J.C., Badiola, E.R., Guillou, H., De La Nuez, J., Pérez Torrado, F.J., 2001. Geology and volcanology of La Palma and El Hierro, Western Canaries. Estud. Geol. 57, 175–273.

Carrol, M.R., Webster, S.D., 1994. Solubilities of Sulphur, noble gases, nitrogen, chlorine and fluorine. Rev. Mineral. 30, 231.

Chaplygin, I.V., Taran, Y.A., Dubinina, E.O., et al., 2015. Chemical composition and metal capacity of magmatic gases of Gorelyi volcano, Kamchatka. Dokl. Earth Sci. 463, 690–694. https://doi.org/10.1134/S1028334X15050104.

Chaplygin, I.V., Lavrushin, V.Y., Dubinina, E.O., Bychkova, Y.V., Inguaggiato, S., Yudovskaya, M.A., 2016. Geochemistry of volcanic gas at the 2012–13 New Tolbachik eruption, Kamchatka. J. Volcanol. Geotherm. Res. 323, 186–193. https://doi.org/10.1016/j.jvolgeores.2016.04.005.

Civico, R., Ricci, T., Scarlato, P., Taddeucci, J., Andronico, D., Del Bello, E., D'Auria, L., Hernández, P.A., Pérez, N.M., 2022. High-resolution digital surface model of the 2021 eruption deposit of Cumbre Vieja volcano, La Palma, Spain. Sci. Data 9, 1–7. https://doi.org/10.1038/s41597-022-01551-8.

D'Auria, L., Koulakov, I., Prudencio, J., Cabrera-Pérez, I., Ibáñez, J.M., Barrancos, J., García-Hernández, R., Martínez van Dorth, D., Padilla, G.D., Przeor, M., Ortega, V., Hernández, P.A., Pérez, N.M., 2022. Rapid magma ascent beneath La Palma revealed by seismic tomography. Sci. Rep. 12, 1–13. https://doi.org/10.1038/s41598-022-21818-9.

Day, J.M., Pearson, D.G., Macpherson, C.G., Lowry, D., Carracedo, J.C., 2010. Evidence for distinct proportions of subducted oceanic crust and lithosphere in HIMU-type mantle beneath El Hierro and La Palma, Canary Islands. Geochim. Cosmochim. Acta 74 (22), 6565–6589. https://doi.org/10.1016/j.gca.2010.08.021.

Day, J.M.D., Troll, V.R., Aulinas, M., Deegan, F.M., Geiger, H., Carracedo, J.C., Gisbert Pinto, G., Perez-Torrado, F.J., 2022. Mantle source characteristics and magmatic processes during the 2021 La Palma eruption. Earth Planet. Sci. Lett. 597, 117793. https://doi.org/10.1016/j.epsl.2022.117793.

Edwards, D.J., Dudhia, A., 1996. Reference Forward Model: High level algorithms definition. In: ESA Doc. POMA-OXF-GS-0004, Eur. Space Agency, Paris.
Esse, B., Burton, M., Hayer, C., La Spina, G., Pardo Cofrades, A., Asensio-Ramos, M., Barrancos, J., Pérez, N., 2025. Forecasting the evolution of the 2021 Tajogaite eruption, La Palma, using satellite-derived SO_2 emission rates. Bull. Volcanol. (under review).
Fernández, J., Escayo, J., Hu, Z., Camacho, A.G., Samsonov, S.V., Prieto, J.F, Tiampo, K. F., Palano, M, Mallorquí, J.J., Ancochea, E. (2021). Detection of volcanic unrest onset in La Palma, Canary Islands, evolution and implications, Sci. Rep. 11, 2540. doi:https://doi.org/10.1038/s41598-021-82292-3.
Francis, P., Burton, M.R., Oppenheimer, C., 1998. Remote measurements of volcanic gas compositions by solar occultation spectroscopy. Nature 396, 567–570. https://doi.org/10.1038/25115.
Gerlach, T.M., Nordie, B.E., 1975. Carbon-Oxygen-Hydrogen-Sulphur gaseous systems. Am. J. Sci. 275, 353–410. https://doi.org/10.1146/annurev.ea.05.050177.000433.
Giggenbach, W.F., 1996. Chemical composition of volcanic gases. In: Scarpa, R., Tilling, R. (Eds.), Monitoring and Mitigation of Volcano Hazard. Springer Verlag, Berlin, Heidelberg, Germany, pp. 221–256.
Giggenbach, W.F., Matsuo, S., 1991. Evaluation of results from 2nd and 3rd IAVCEI field workshops on volcanic gases, Mt. Usu, Japan, and White Island, New Zealand. Appl. Geochem. 6, 125–141. https://doi.org/10.1016/0883-2927(91)90024-J.
Giggenbach, W.F., Shinohara, H., Kusakabe, M., Ohba, T., 2005. Formation of acid volcanic brines through interaction of magmatic gases, seawater, and rock within the White Island volcanic-hydrothermal system, New Zealand. In: Simmons, S.F., Graham, I. (Eds.), Volcanic, Geothermal, and Ore-Forming Fluids: Rulers and witnesses of Processes within the Earth, GeoScienceWorld. https://doi.org/10.5382/SP.10.02.
Gonnermann, H., Taisne, B., 2015. Magma transport in dikes, Second ed. Elsevier Inc. https://doi.org/10.1016/b978-0-12-385938-9.00010-9
Gordon, I.E., et al., 2020. The HITRAN 2020 molecular spectroscopic database. J. Quantit. Spectr. Radiat. Transf. 277, 107949.
Guillou, H., Carracedo, J.C., Duncan, R.A., 2001. K–ar, 40ar–39ar ages and magnetostratigraphy of Brunhes and Matuyama lava sequences from La Palma Island. J. Volcanol. Geotherm. Res. 106, 175–194. https://doi.org/10.1016/s0377-0273(00)00294-8.
Halldórsson, S.A., Marshall, E.W., Caracciolo, A., Matthews, S., Bali, E., Rasmussen, M.B., Ranta, E., Gunnarsson Robin, J., Guðfinnsson, G.H., Sigmarsson, O., Maclennan, J., Jackson, M.G., Whitehouse, M.J., Jeon, H., van der Meer, Q.H.A., Mibei, G.K., Kalliokoski, M.H., Repczynska, M.M., Rúnarsdóttir, R.H., Sigurðsson, G., Pfeffer, M. A., Scott, S.W., Kjartansdóttir, R., Kleine, B.I., Oppenheimer, C., Aiuppa, A., Ilyinskaya, E., Bitetto, M., Giudice, G., Stefánsson, A., 2022. Rapid shifting of a deep magmatic source at Fagradalsfjall volcano, Iceland. Nature 609, 529–534. https://doi.org/10.1038/s41586-022-05036-9.
Hoernle, K., Zhang, Y.-S., Graham, D., 1995. Seismic and geochemical evidence for large-scale scale mantle upwelling beneath the eastern Atlantic and western and Central Europe. Nature 374, 34–39. https://doi.org/10.1038/374034a0.
Holloway, J.R., Blank, J.G., 1994. Application of experimental results to C-O-H species in natural melts. In: Volatiles in Magmas, 30, pp. 187–230.
Jaupart, C., Vergniolle, S., 1988. Laboratory models of Hawaiian and Strombolian eruptions. Nature 331, 58–60. https://doi.org/10.1038/331058a0.
Jimenez-Mejias, M., Andujar, J., Scaillet, B., Casillas, R., 2021. Experimental determination of H_2O and CO_2 solubilities of mafic alkaline magmas from Canary Islands. Compt. Rendus Geosci. 353. https://doi.org/10.5802/crgeos.84.
La Spina, A., Burton, M., Salerno, G.G., 2010. Unravelling the processes controlling gas emissions from the central and northeast craters of Mt. Etna. J. Volcanol. Geotherm. Res. 198, 368–376. https://doi.org/10.1016/j.jvolgeores.2010.09.018.
La Spina, A., Burton, M., Allard, P., Alparone, S., Muré, F., 2015. Open-path FTIR spectroscopy of magma degassing processes during eight lava fountains on Mount Etna. Earth Planet. Sci. Lett. 413, 123–134. https://doi.org/10.1016/j.epsl.2014.12.038.
La Spina, A., Burton, M., Salerno, G., Caltabiano, T., 2023. Insights into magma dynamics at Etna (Sicily) from SO_2 and HCl -fluxes during the 2008–2009 eruption. Geology 51, 419–423. https://doi.org/10.1130/g50707.1.
La Spina, A., Burton, M., Houghton, B.F., Sutton, A.J., Esse, B., 2024. Magmatic degassing dynamics at Halema'uma'u Crater, Kīlauea, Hawaii. Earth Planet. Sci. Lett. 648, 119062. https://doi.org/10.1016/j.epsl.2024.119062.
Longpré, M.A., Stix, J., Klügel, A., Shimizu, N., 2017. Mantle to surface degassing of carbon- and Sulphur-rich alkaline magma at El Hierro, Canary Islands. Earth Planet. Sci. Lett. 460, 268–280. https://doi.org/10.1016/j.epsl.2016.11.043.
Lundstrom, C.C., Hoernle, K., Gill, J., 2003. U-series disequilibria in volcanic rocks from the Canary Islands: Plume versus lithospheric melting. Geochim. Cosmochim. Ac 67 (21), 4153–4177. https://doi.org/10.1016/S0016-7037(03)00308-9.
Masson, D.G., Watts, A.B., Gee, M.J.R., Urgeles, R., Mitchell, N.C., Le Bas, T.P., Canals, M., 2002. Slope failures on the flanks of the Western Canary Islands. Earth Sci. Rev. 57, 1–35. https://doi.org/10.1016/s0012-8252(01)00069-1.
Métrich, N., Allard, P., Aiuppa, A., Bani, P., Bertagnini, A., Shinohara, H., Parello, F., Di Muro, A., Garaebiti, E., Belhadj, O., 2011. Magma and volatile supply to post-collapse volcanism and block resurgence in Siwi Caldera (Tanna Island, Vanuatu Arc). J. Petrol. 52, 1077–1105. https://doi.org/10.1093/petrology/egr019.
Mizutani, Y., Sugiura, T., 1982. Variations in chemical and isotopic compositions of fumarolic gases from Showashinzan volcano, Hokkaido, Japan. Geochem. J. 16, 63–71. https://doi.org/10.2343/geochemj.16.63.
Mizutani, Y., Hayashi, S., Sugiura, T., 1986. Chemical and isotopic compositions of fumarolic gases from Kuju-Iwoyama, Kyushu, Japan. Geochem. J. 20, 273–285. https://doi.org/10.2343/geochemj.20.273.
Moretti, R., Papale, P., Ottonello, G., 2003. A model for the saturation of C-O-H-S fluids in silicate melts. Geol. Soc. Spec. Publ. 213, 81–101. https://doi.org/10.1144/GSL.SP.2003.213.01.06.
Moussallam, Y., Longpré, M.A., McCammon, C., Gomez-Ulla, A., Rose-Koga, E.F., Scaillet, B., Peters, N., Gennaro, E., Paris, R., Oppenheimer, C., 2019a. Mantle plumes are oxidised. Earth Planet. Sci. Lett. 527, 115798. https://doi.org/10.1016/j.epsl.2019.115798.
Moussallam, Y., Oppenheimer, C., Scaillet, B., 2019b. On the relationship between oxidation state and temperature of volcanic gas emissions. Earth Planet. Sci. Lett. 520, 260–267. https://doi.org/10.1016/j.epsl.2019.05.036.
Navarro, J.M., Coello, J., 1993. Sucesión de episodios en la evolución geológica de La Palma. Mapa geológico de La Palma, ICONA, Madrid.
Nicklas, R.W., Hahn, R.K.M., Willhite, L.N., Jackson, M.G., Zanon, V., Arevalo Jr., R., Day, J.M.D., 2022a. Oxidized mantle sources of HIMU- and EM-type Ocean Island Basalts. Chem. Geol. 602, 120901. https://doi.org/10.1016/j.chemgeo.2022.120901.
Nicklas, R.W., Hahn, R.K.M., Day, J.M.D., 2022b. Oxidation of La Réunion lavas with MORB-like fO_2 by assimilation. Geochem. Perspect. Lett. 20, 32–36. https://doi.org/10.7185/geochemlet.2205.
Oppenheimer, C., Kyle, P.R., 2008. Probing the magma plumbing of Erebus volcano, Antarctica, by open-path FTIR spectroscopy of gas emissions. J. Volcanol. Geotherm. Res. 177 (3), 743–754. https://doi.org/10.1016/j.jvolgeores.2007.08.022.
Oppenheimer, C., Lomakina, A.S., Kyle, P.R., Kingsbury, N.G., Boichu, M., 2009. Earth Planet. Sci. Lett. 284 (3–4), 392–398. https://doi.org/10.1016/j.epsl.2009.04.043.
Oppenheimer, C., Scaillet, B., Woods, A., Sutton, A.J., Elias, T., Moussallam, Y., 2018. Influence of eruptive style on volcanic gas emission chemistry and temperature. Nat. Geosci. 11, 678–681. https://doi.org/10.1038/s41561-018-0194-5.
Padrón, E., Pérez, N.M., Rodríguez, F., Melián, G.V., Hernández, P.A., Sumino, H., Padilla, G.D., Barrancos, J., Dionis, S., Notsu, K., Calvo, D., 2015. Dynamics of diffuse carbon dioxide emissions from Cumbre Vieja volcano, La Palma, Canary Islands. Bull. Volcanol. 77, 28. https://doi.org/10.1007/s00445-015-0914-2.
Padrón, E., Pérez, N.M., Hernández, P.A., Sumino, H., Melián, G.V., Alonso, M., Rodríguez, F., Asensio-Ramos, M., D'Auria, L., 2022. Early precursory changes in the $^3He/^4He$ ratio prior to the 2021 Tajogaite eruption at Cumbre Vieja volcano, La Palma, Canary Islands. Geophys. Res. Lett. 49. https://doi.org/10.1029/2022GL099992 e2022GL099992.
Pankhurst, M.J., Scarrow, J.H., Barbee, O.A., Hickey, J., Coldwell, B.C., Rollinson, G.K., Rodríguez-Losada, J.A., Martín-Lorenzo, A., Rodríguez, F., Hernández, W., Calvo Fernández, D., Hernández, P.A., Pérez, N.M., Sánchez, F., 2022. Rapid response petrology for the opening eruptive phase of the 2021 Cumbre Vieja eruption, La Palma, Canary Islands. Volcanica 5, 1, 11.21223/rs.3.rs-963593/v1.
Pfeffer, M.A., Bergsson, B., Barsotti, S., Stefánsdóttir, G., Galle, B., Arellano, S., Conde, V., Donovan, A., Ilyinskaya, E., Burton, M., Aiuppa, A., Whitty, R.C.W., Simmons, I.C., Arason, Þ., Jónasdóttir, E.B., Keller, N.S., Yeo, R.F., Arngrímsson, H., Jóhannsson, Þ., Butwin, M.K., Askew, R.A., Dumont, S., Von Löwis, S., Ingvarsson, Þ., La Spina, A., Thomas, H., Prata, F., Grassa, F., Giudice, G., Stefánsson, A., Marzano, F., Montopoli, M., Mereu, L., 2018. Ground-based measurements of the 2014–2015 Holuhraun volcanic cloud (Iceland). Geosciences 8, 29. https://doi.org/10.3390/geosciences8010029.
Pfeffer, M.A., Arellano, S., Barsotti, S., Petersen, G.N., Barnie, T., Ilyinskaya, E., Hjörvar, T., Bali, E., Pedersen, G.B.M., Guðmundsson, G.B., Vogfjorð, K., Ranta, E.J., Óladóttir, B.A., Edwards, B.A., Moussallam, Y., Stefánsson, A., Scott, S.W., Smekens, J.-F., Varnam, M., Titos, M., 2024. SO_2 emission rates and incorporation into the air pollution dispersion forecast during the 2021 eruption of Fagradalsfjall, Iceland. J. Volcanol. Geotherm. Res. 449, 108064. https://doi.org/10.1016/j.jvolgeores.2024.108064.
Priatna, P., Kadarsetia, E., 2007. Characteristics of volcanic gas correlated to the eruption activity; Case study in the Merapi Volcano, periods of 1990-1994. Indonesian J. Geosci. 2, 235–246. https://doi.org/10.17014/ijog.2.4.235-246.
Ranta, E., Halldórsson, S.A., Barnes, J.D., Jónasson, K., Stefánsson, A., 2020. Chlorine isotope ratios record magmatic brine assimilation during rhyolite genesis. Geochem. Perspect. Lett. 16, 35–39. https://doi.org/10.7185/geochemlet.2101.
Romero, J.E., Burton, M., Cáceres, F., Taddeucci, J., Civico, R., Ricci, T., Pankhurst, M.J., Hernández, P.A., Bonadonna, C., Llewellin, E.W., Pistolesi, M., Polacci, M., Solana, C., D'Auria, L., Arzilli, F., Andronico, D., Rodríguez, F., Asensio-Ramos, M., Martín-Lorenzo, A., Hayer, C., Scarlato, P., Pérez, N.M., 2022. The initial phase of the 2021 Cumbre Vieja ridge eruption (Canary Islands): products and dynamics controlling edifice growth and collapse. J. Volcanol. Geotherm. Res. 431. https://doi.org/10.1016/j.jvolgeores.2022.107642.
Rosenthal, A., Hauri, E.H., Hirschmann, M.M., 2015. Experimental determination of C, F, and H partitioning between mantle minerals and carbonated basalt, CO_2/Ba and CO_2/Nb systematics of partial melting, and the CO_2 contents of basaltic source regions. Earth Planet. Sci. Lett. 412, 77–87. https://doi.org/10.1016/j.epsl.2014.11.044.
Sawyer, G.M., Carn, S.A., Tsanev, V., Oppenheimer, C., Burton, M., 2008. Investigation into magma degassing at Nyiragongo volcano, Democratic Republic of the Congo. Geochem. Geophys. Geosyst. 9. https://doi.org/10.1029/2007GC001829. Q02017.
Sawyer, G.M., Salerno, G.G., Le Blond, J.S., Martin, R.S., Spampinato, L., Roberts, T.J., Mather, T.A., Witt, M.L.I., Tsanev, V.I., Oppenheimer, C., 2011. Gas and aerosol emissions from Villarrica volcano, Chile. J. Volcanol. Geotherm. Res. 203, 62–75. https://doi.org/10.1016/j.jvolgeores.2011.04.003.
Schmincke, H.-U., Sumita, M., 2004. Geological Evolution of the Canary Islands: A Young Volcanic Archipelago Adjacent to the Old African Continent. Görres-Verlag, Koblenz. ISBN 978-3-86972-005-0.
Scott, S., Pfeffer, M., Oppenheimer, C., Bali, E., Lamb, O.D., Barnie, T., Woods, A.W., Kjartansdóttir, R., Stefánsson, A., 2023. Near-surface magma flow instability drives

cyclic lava fountaining at Fagradalsfjall, Iceland. Nat. Commun. 14, 1–9. https://doi.org/10.1038/s41467-023-42569-9.

Shinohara, H., 2013. Volatile flux from subduction zone volcanoes: Insights from a detailed evaluation of the fluxes from volcanoes in Japan. J. Volcanol. Geotherm. Res. 268, 46–63. https://doi.org/10.1016/j.jvolgeores.2013.10.007.

Shinohara, H., Giggenbach, W.F., Kazahaya, K., Hedenquist, J.W., 1993. Geochemistry of volcanic gases and hot springs of Satsuma-Iwojima, Japan - following Matsuo. Geochem. J. 27, 271–285. https://doi.org/10.2343/geochemj.27.271.

Sparks, R.S.J., Barclay, J., Jaupart, C., Mader, H.M, Phillips, J.C. (1994). Physical aspects of magma degassing I: Experimental theoretical constraints on vesiculation. In: Volatiles in Magmas, Carroll, M.R., Holloway, J.R. (Eds), Reviews in Mineralogy, Mineralogical Society of America, v.30, 509 pp.

Spilliaert, N., Métrich, N., Allard, P., 2006. S-Cl-F degassing pattern of water-rich alkali basalt: modelling and relationship with eruptive styles on Mount Etna volcano. Earth Plan. Sci. Lett. 248, 772–786.

Staudigel, H., Feraud, G., Giannerini, G., 1986. The history of intrusive activity on the island of La Palma (Canary Islands). J. Volcanol. Geotherm. Res. 27, 299–322. https://doi.org/10.1016/0377-0273(86)90018-1.

Staudigel, H., Schmincke, H.-U., 1984. The Pliocene seamount series of La Palma/Canary Islands. J. Geophys. Res. 89, 11195–11215. https://doi.org/10.1029/JB089iB13p11195.

Symonds, R.B., Rose, W.I., Gerlach, T.M., Briggs, P.H., Harmon, R.S., 1990. Evaluation of gases, condensates, and SO2 emissions from Augustine Volcano, Alaska - The degassing of a Cl-rich volcanic system. Bull. Volcanol. 52 (5), 355–374. https://doi.org/10.1007/BF00302048.

Taracsák, Z., Hartley, M.E., Burgess, R., Edmonds, M., Iddon, F., Longpré, M.A., 2019. High fluxes of deep volatiles from ocean island volcanoes: Insights from El Hierro, Canary Islands. Geochim. Cosmochim. Acta 258, 19–36. https://doi.org/10.1016/j.gca.2019.05.020.

Taracsák, Z., Longpré, M.A., Tartèse, R., Burgess, R., Edmonds, M., Hartley, M.E., 2022. Highly oxidising conditions in volatile-rich El Hierro magmas: implications for ocean island magmatism. J. Petrol. 63. https://doi.org/10.1093/petrology/egac011 egac011.

Torres-González, P.A., Luengo-Oroz, N., Lamolda, H., D'Alessandro, W., Albert, H., Iribarren, I., Moure-García, D., Soler, V., 2020. Unrest signals after 46 years of quiescence at Cumbre Vieja, La Palma, Canary Islands. J. Volcanol. Geotherm. Res. 392, 106757. https://doi.org/10.1016/j.jvolgeores.2019.106757.

Ubide, T., Márquez, A., Ancochea, E., Huertas, M.J., Herrera, R., Coello-Bravo, J.J., Sanz-Mangas, D., Mulder, J., MacDonald, A., Galindo, I., 2023. Discrete magma injections drive the 2021 La Palma eruption. Sci. Adv. 9, eadg4813. https://doi.org/10.1126/sciadv.adg4813.

Wadsworth, F.B., Llewellin, E.W., Farquharson, J.I., Gillies, J.K., Loisel, A., Frey, L., Ilyinskaya, E., Thordarson, T., Tramontano, S., Lev, E., Pankhurst, M.J., Galdeano Rull, A., Asensio-Ramos, M., Pérez, N.M., Hernández, P.A., Calvo, D., Solana, M.C., Kueppers, U., Polo Santabárbara, A., 2022. Crowd-sourcing observations of volcanic eruptions during the 2021 Fagradalsfjall and Cumbre Vieja events. Nat. Commun. 13, 1–5. https://doi.org/10.1038/s41467-022-30333-4.

Walowski, K.J., Kirstein, L.A., DeHoog, J.C.M., Elliott, T.R., Savov, I.P, Jones, R.E. (2019). Investigating ocean island mantle source heterogeneity with boron isotopes in melt inclusions. Earth Plan. Sci. Lett., 508, 97–108. doi:https://doi.org/10.1016/j.epsl.2018.12.005.

Zanon, V., Schiavi, F., Cyrzan, K., Pankhurst, M.J., 2024. Toward a near real-time magma ascent monitoring by combined fluid inclusion barometry and ongoing seismicity. Sci. Adv. 10, eadi4300. https://doi.org/10.1126/sciadv.adi4300.

Zelenski, M., Taran, Y., 2011. Geochemistry of volcanic and hydrothermal gases of Mutnovsky volcano, Kamchatka: evidence for mantle, slab, and atmosphere contributions to fluids of a typical arc volcano. Bull. Volcanol. 73, 373–394. https://doi.org/10.1007/s00445-011-0449-0.